Quantitative measurements of preferential evaporation effects of multicomponent gasoline fuels sprays at ECN Spray G conditions

Matthieu Cordier, Lama Itani, Gilles Bruneaux

Quantitative measurements of preferential evaporation effects of multicomponent gasoline fuels sprays at ECN Spray G conditions

Matthieu Cordier[1], Lama Itani[1], Gilles Bruneaux[1]

[1] IFP Energies nouvelles, 92852 Rueil-Malmaison Cedex, France; Institut Carnot IFPEN Transports Energie

Abstract

A Two Tracers Laser-Induced Fluorescence (2 TLIF) technique is used to quantify the effects of preferential evaporation of multi-component fuels on the fuel component distribution. The technique is based on the simultaneous detection of the fluorescence of two aromatic tracers with complementary evaporation characteristics matched to different components of a multi-component fuel. Relative variations in the spatial distribution of tracer distribution as a consequence of preferential evaporation are determined from the ratio of LIF-signals measured within two distinct spectral bands. A thermodynamic model is then used to relate the ratio map with the fuel component map. The accuracy and precision of the method are characterized from determining the LIF-signal ratio within two identical spectral bands. Measurements are performed in a high-pressure high-temperature vessel equipped with a 8 holes injector. The ECN Spray G target conditions are chosen as reference conditions at injection. The only difference with these target conditions is the use of a multicomponent surrogate fuel. Parametric variations around these target conditions are also performed in order to investigate their effect on the preferential evaporation effect. The ambient temperature is varied between 525 and 625K and the injection pressure is reduced from 200 to 100bar. The impact of ethanol addition is also study with two different fuel mixtures in addition to the reference surrogate fuel: E20 and E85 which feature 20 and 85% of pure ethanol within surrogate, respectively. A significant preferential evaporation effect is observed in this condition representative of engine applications, and results in a spatial segregation between low and high volatility fuel components, respectively at the tail and tip of the plumes. This effect is enhanced by the addition of ethanol, the decrease of ambient temperature and of injection pressure.

Keywords

Multi-component fuels; ECN; Spray G; gasoline sprays; preferential evaporation; laser-induced fluorescence; E20; E85.

1. Introduction

Energy conversion based on fossils fuel is at the origin of significant greenhouse gases (CO_2) emissions. Due to the share of CO_2 emission from the transport domain, the efficiency of combustion system has to be significantly increased to reduce the impact on global warming. In addition, to limit the effect of transport on human health, pollutant emission standards are currently more and more stringent, in particular concerning pollutants such as NOx or particles emissions which depend on combustion quality.

Gasoline engine underwent a profound evolution in the last decades to meet these targets. For this purpose, the use of Gasoline Direct injection (GDI) technology is becoming a standard thanks to its ability to reduce fuel consumption and pollutant emissions by improving air fuel mixing[1] and allowing a better control of the combustion.. In addition, advanced combustion strategy, such as stratified combustion, can be implemented to further improve efficiency by running the engine at globally lean conditions[2]. This type of combustion is not only influenced by the spray structure but also by the evaporation process. In parallel the global trend is also to improve the well-to-wheel balance[3,4] using fuels from renewable origin. For instance the mixture of gasoline with a fixed share of ethanol (10% in volume) is now a standard in Europe, and the share of renewable fuels is bound to further increase in the future. This evolution of the fuel composition must be taken into account during the design of combustion systems since it may significantly affect the evaporation and the mixing process. In particular it has been shown that the mixture of gasoline and ethanol displays a specific azeotropic behavior[5–8]. Engines designed to use E85 (85% of ethanol in volume) so called flex fuel engine[9,10] are also developed, requiring specific tuning.

Most of these improvements aiming at increasing engine efficiency and reducing engine out pollutant emission greatly affect the injection process. Since atomization, evaporation and mixing determine the efficiency of combustion, it is of first interest to deeply understand how direct injection[1] and biofuel will influence these physical phenomena[6]. One of the processes of interest is the preferential evaporation of multicomponent fuel[11,12]. The latter happen when low and high volatility fuel components evaporate at different rates in the combustion chamber. This may lead to inhomogeneous distribution of the fuel components in the combustion chamber, therefore impacting local flame propagation, pollutant formation and possibly auto-ignition properties.

To insure the efficient development of future combustion system, these physical processes that are more and more complex have to be well taken into account by the numerical simulation tools used in the development process. To obtain such predictive models, validation against experimental data is essential. Today, integration of preferential evaporation effect in Computational Fluid Dynamic (CFD) codes is still challenging [6] because of the lack of validation data available. Therefore it is of first importance to develop quantitative measurement techniques able to account for this preferential evaporation effect. In this context, laser induced fluorescence (LIF) techniques are commonly used to characterize the spatial distribution of particular species [13–16]. LIF is a two dimensional technique based on the excitation of a fluorescent

molecule (the tracer) with a laser followed by light emission at specific wavelength, depending on the tracer. Recently, this technique has been adapted to the quantification of preferential evaporation of a multicomponent fuel by determining the ratio of low/high volatility components of the fuel with the imaging of two tracer[17,12,11]. Only few references are available in the literature concerning the application of this technique[18,19,15,20]. In addition, cross-talk phenomena have to be well taken into account in order to avoid strong limitations of the technique[21]. Once the local tracer concentration is obtained, another challenge is to relate it to the local fuel vapor composition. This requires the use of an accurate thermodynamic model[6]. Such a model was recently developed by Bardi et al.[20] and validated against experimental data. Its purpose is to provide information on the evolution of fuel components and tracer distilled fraction during the evaporation process.

In this context, the purpose of the work presented here was to use the two tracers LIF technique and the thermodynamic model respectively developed in[12] and[20] to perform quantitative measurements of preferential evaporation effects of multicomponent gasoline fuels sprays at Engine Combustion Network (ECN) Spray G conditions[22]. Variations of operating conditions including ambient temperature, injection pressure and fuel mixture composition (ethanol addition) were also performed to address their effect on the evaporation process.

The paper first presents the experimental methodology, then the results of 2 Tracer LIF measurements. A discussion part where the results are analyzed and interpreted follows.

2. Methodology

Commercial gasoline fuels are composed of hundreds of different species, some of which being fluorescent under laser excitation[23]. Since these later species are unknown, it is difficult to obtain quantitative information when directly exciting the fluorescence of the fuel. Surrogate fuels, designed to be transparent to laser excitation and representative of the evaporation of the real fuel, doped with fluorescent tracers of know properties are therefore used to bypass this difficulty. Such a surrogate fuel composed of isooctane, undecane and pentane was designed in[20] using a thermodynamic approach. It matches very well the evaporation characteristics of commercial gasoline fuels. This surrogate is non-fluorescent to laser excitation, enabling the addition of two fluorescent tracers with complementary evaporation and spectral characteristics. The selection of these two tracers was made taking into account their evaporation and fluorescence characteristics. High quantum yields tracers with minimum cross-talk were chosen. P-difluorobenzene and 1-methylnaphtalene were therefore selected to respectively trace high volatility components (isooctane and pentane) and low volatility component (undecane)[20,12,17]. These tracers feature well separated fluorescent spectra which enable simultaneous accurate measurements with minimum cross-talk pollution [12,24]. In the absence of preferential evaporation, both tracers would appear at a fixed concentration ratio throughout the fuel cloud and the LIF-signal ratio of both tracers

would be constant within the entire field of view. Deviations from an homogeneous unity value, thus, directly indicate regions where preferential evaporation affects the fuel homogeneity. The following sections detail how this methodology was implemented.

a. Experimental setup

Measurements of the vapor fuel distributions have been performed in an optically accessible high-pressure high-temperature (HPHT) pre-combustion vessel (Figure 1~~Figure 1~~, left) in conditions relevant for IC engine injection,. The vessel operation is extensively described in previous studies[25], and it is only briefly summarized here. Two cylindrical sapphire windows on opposite sides of the vessel provide a field of view of 85×85 mm^2 while two 65×10 mm^2 quartz windows provide laser access perpendicularly to the viewing direction. High temperature and pressure prior to the start of injection are provided by pre-combustion of a $C_2H_2/H_2/O_2/N_2$ mixture. After this pre-combustion, gases gradually cool down and the fuel is injected after a specific delay when the desired temperature and pressure are reached. For all experiments presented in this paper, the mixture proportion was fixed so that no O_2 was left after pre-combustion to prevent for fluorescence quenching and spray ignition.

FIG1

Figure 1: high pressure high temperature (HPHT) vessel (top) and optical arrangement for two tracers LIF technique (bottom).

For LIF measurements, the fourth harmonic of a Nd:YAG laser (266 nm) was used to form a light-sheet (52×0.3 mm^2) that is passed through the center of the fuel jet, with the top of the sheet 12 mm away from the injector tip due to injector position and optical accessibility. LIF signals were acquired with a fast achromatic UV lens (f = 45 mm, $f_\#$ = 1.8, EADS Sodern) coupled with an image doubler (LaVision) and imaged onto a single ICCD camera (Princeton PI-MAX, 512×512 pixels). Details of the optical arrangement are given in Figure 1~~Figure 1~~. Two different filter configurations were used for the two channels of the image doubler: *Configuration A* was employed to assess preferential evaporation by simultaneously collecting the signal of both tracers on either channel. The filters used for the detection of *p*-difluorobenzene and 1-methylnaphthalene LIF were 292±14 nm and 340±14 nm (both: Semrock, transmissivity >70%), respectively. This configuration requires the exact superposition (mapping) of both images to generate a meaningful image of the intensity ratio (S_{292}/S_{340}). *Configuration B* was used for optimizing the image mapping, assessing the accuracy and precision, and calibrating relative sensitivities[12,17]. Two identical filters (292±14 nm) were placed on both sides of the image stereoscope and the ratio of the nominally identical images (S_{292}/S_{292}) allows to assess experimental limitations.

b. Injector

The injector mounted on the HPHT vessel is the “Spray G” of the ECN framework[22]. The operating conditions correspond to a non-reacting early injection case for spray-guided gasoline injection. Its specifications are for modern advanced injection

systems with high pressure capability. Spray G is generated by a solenoid eight-hole injector which results in a full-cone spray structure. It represents the majority of gasoline injector currently used and was fully characterized in terms of nozzle geometry, initial and boundary spray conditions within the ECN framework[22]. The LIF technique used in this study is based on tracer excitation in the vapor phase. Figure 2~~Figure 2~~ presents light-sheet position regarding to spray plumes. Plumes, coming from eight holes of the injector, are numbered from 1 to 8 and diagnostics are done on plume 2 and 6. The presence of liquid droplets should be avoided. Mie-scattering was performed to check for droplet presence in the field of view, at the acquisition time. The results showed that the spray is fully evaporated at 3ms after start of injection for this injector for the conditions investigated.

FIG2

Figure 2: spray orientation used for LIF imaging The plumes originating from 8 individual holes of Spray G are numbered from 1 to 8 based on the ECN reference numeration. The green arrow indicates the direction of the laser-light sheet and the visualized spray pair 2-6.

c. Data processing

i. Ratio image post-processing

The post processing methodology developed in[12,17] was applied in the present configuration. The two-tracer LIF method requires the simultaneous measurement of emission intensities associated with each tracer in the fuel mixture. Preferential evaporation is determined from the LIF intensity ratio obtained from the combined images from *Configuration A*. Both channels were flat-field corrected by dividing the raw images by measurements of average homogeneous images with *Configuration B*. These homogeneous images were obtained by performing 10 injections of surrogate/tracer mixture in the HPHT vessel, in an environment composed of N_2 at 7 bar, followed by 5 to 10 seconds with the mixing fan on to ensure homogenous mixing. Background correction is also done on every image, by subtraction of the average background image from LIF images. The background image was acquired by averaging 20 instantaneous images obtained while the laser is running and with only N2 flowing in the cell. The image was then splited into two separate images, one representing the LIF signal at 292±14 nm (S_{292}) and the other representing the LIF signal at 340±14nm (S_{340}). A threshold of 10% was applied to both images to limit the determination of the signal ratio to regions with sufficient signal-to-noise ratios. A 5×5 pixel (i.e., 2×2 mm²) median filter was applied to the individual images to reduce shot noise. In addition, correction for trace impurities present in the surrogate fuel and for fluorescence cross talk between the tracers is applied. These corrections are described in more detail in section 4. After mapping the LIF images, the LIF-signal ratio image was calculated for each single laser shot. An average image was then obtained from 25 measurements at least. More details about data processing can be found in[17,11]. Finally, it is important to note that no correction of the LIF signal by the temperature distribution was required in this experiment since it has been previously shown in ref.[17] that the temperature gradients in the plumes at this late

timing are low and result in negligible corrections of the LIF signal from fluorescence thermal quenching.

ii. Composition map

The 2 tracer LIF measurement technique provides quantitative information on the ratio of local tracer concentration. The later can be combined with the results of the thermodynamic model to derive information on the local composition of the fuel components, since the thermodynamic model provides the evaporation characteristics of the fuel components along with the tracer.

This link between the measured ratio field and the fuel composition is realized by deriving composition maps from the evaporation diagram obtained by thermodynamic modeling. More details about this derivation and the related uncertainties are developed in[20]. It is important to note that since the thermodynamic model represents a simplified configuration compared to the evaporation of a spray, the use of this composition map to derive fuel component distribution information from measured ratio maps is subject to the main following hypothesis:

- It is assumed that the evaporation at the liquid-vapor interface is at equilibrium
- Preferential diffusion within the liquid droplet and in the gas phase are neglected
- A simplified model for the spray evaporation process is considered

More discussions of these hypothesis are available in ref[20].

d. Determination of measurement uncertainties

The uncertainty analysis developed in[12,17] was applied here. In order to ensure quantitative measurements of the preferential evaporation a set of verifications have been carried out to optimize and then determine the precision and accuracy of the measurement.
First, although non-fluorescing components were selected in the composition of the surrogate fuel, residual fluorescence signal due to impurity may still occur. This contribution was characterized by performing LIF spray imaging without fluorescence tracer and was taken into account in the image post processing[12], by reducing the signal S292 of 8%. S340 is very little impacted by residual fluorescence and no correction is needed. Although tracer with minimal cross talk have been selected, the signal of p-difluorobenzene and 1-methylnaphthalene to the respective other channel was determined and accounted for in the evaluation of preferential evaporation. Thus, 8% of the S292 intensity was subtracted from S340 and 6% of the S340 intensity was subtracted from S292. [17]. Besides these errors sources, other which may affect the ratio quantification are:

- Image superposition: to calculate accurately the ratio of fluorescence signal coming from the two channels, a transformation matrix is determined. This transformation consists in applying translation, rotation

and scaling to one image. It is obtain with configuration B. Image coming from the first channel serves as reference and the image coming from second channel undergoes transformation. Optimum matrix parameters are obtained when standard deviation of the signal intensity correlation for image pair is minimum.

- Flat field correction: pixel sensitivity is not homogeneous on the CCD sensor and it contributes to dispersion of the signal intensity. To evaluate this inhomogeneity, LIF images are acquired in homogeneous conditions in the HPHT vessel. Both images should be identical in theory, but this is not the case in practice. The average LIF-ratio image was then determined and used as a correction image. By multiplying the LIF images (in configuration A) by this correction image, the measurement precision is increased.

- Shot noise: this random error affects all imaging system and can only be minimized by spatial averaging (then at the cost of a loss of spatial resolution).

Once these correction are taken into account to minimize the measurement error, the latter was determined experimentally according to the methodology developed in[17,12] by performing an analysis of images obtained in configuration B. In the latter, the nominal characteristics of the two collection paths are identical so that in theory the exact same image should be obtained and the corresponding ratio should be unity everywhere. However the error source mentioned above affect the collection resulting in deviation from unity. The latter can be used to determine the effect of these error sources on the ratio measurement. Indeed, since these error sources affect the image in configuration B similarly to the ones obtained in configuration A, the analysis of the deviation from unity of the ratio images obtained in configuration B provides information on the accuracy and the measurement uncertainty.

The remaining error can be attributed to shot noise and to the imperfect correction of the other sources. The determination of the systematic error (accuracy) is based on the analysis of the average images while that of the measurement uncertainty is based on the analysis of the individual images.

e. Configurations under investigation

The ECN Spray G experimental conditions were selected for these measurements. The injection pressure and injection duration were 200 bar and 950 µs respectively and the ambient density was 3.5 kg/m^3.These target conditions reproduce modern gasoline direct injection conditions. They correspond almost exactly to the spray G conditions target, except for the fuel: instead of the single component iso-octane fuel recommended for ECN Spray G conditions, in our case a multicomponent fuel mixture is injected to study preferential evaporation effects. At the injection timing, oxygen-free environment enable to prevent from fluorescence quenching.

In the framework of the study, different parameters have been varied in order to study their effect on differential evaporation. First of all, three different fuels were tested: surrogate, E20 and E85. The two latter are respectively a mixture of surrogate with 20% and 85% of ethanol, in volume. For each fuel, the ambient temperature T_{amb} inside the vessel was varied between 525 and 625K in order to study the effect of temperature on preferential evaporation. The effect of injection pressure P_{inj} was also investigated for the surrogate fuel only. The reference image timing after start of injection (ASOI) is 4ms. This timing was selected using the Mie scattering image to ensure that sufficient time is available after the end of injection so that all the fuel is evaporated. For each configuration, average results are obtained from 25 consecutive tests, at least.

Fuel	Visualization time (ms, ASOI)	T_{amb} (K)			P_{inj} (bar)
		525	573	625	
Surrogate	4	X	X*	X	200
	4			X	100
E20	4	X	X	X	200
E85	4	X	X	X	200

Table 1: configurations under investigation (*: indicate reference spray G ECN condition).

3. Results

In this section, the results obtained with the two tracers LIF technique for the different conditions under investigations are presented.

a. Accuracy and measurement uncertainty

As presented in section 2.d, the images obtained in configuration B provide a unique framework for the determination of the measurement accuracy and uncertainty. In theory, without error sources all the images obtained in configuration B should be equal to 1 everywhere where fluorescence is collected. Therefore any deviation from unity provides a quantitative information on the effect of error sources on the ratio measurement. The measurement accuracy is determined from the analysis of the average images while the measurement uncertainty is determined from the analysis of the set of individual images.

Figure 3~~Figure 3~~ presents the average isofilter image obtained in this configuration for the surrogate fuel at the reference condition: ambient temperature of 573K and injection pressure of 200bar. It can be clearly observed on the image that the average ratio of fluorescence is close to unity. The value obtained when averaging the

image is 1.01 for a target value of 1, indicating that the global accuracy of the measurement is high. The standard deviation of this image is 0.06, indicating the local measurement accuracy when considering a given position in the plumes. The latter is the result of lack of statistics and imperfect correction of image registration and flat field correction. The standard deviation of 0.06 obtained here is lower than the one obtained in the work of Itani et al.[11] indicating a better accuracy. This improvement is mainly due to an upgrade of the stereoscope used for the acquisition. The new model significantly improves the image quality and reduces vignetting effects.

Figure 4 presents an image of the measurement uncertainty of the results in the same conditions. The uncertainty refers to the 95% confidence interval, computed with the set of individual images using the Student's t-distribution for each pixel of the image[26]. The image shows that the measurement uncertainty is less than 0,02 in the central part of the plumes and increases to approximately 0,15 in a band located at the edges because of the higher fluctuations.

For the subsequent investigation, the images will be analyzed as follow

- If the ratio variation is lower than the measurement accuracy (0.06) added with the measurement uncertainty (0.02 in the central part of the plumes and 0.15 on the edges) it will be considered as not significant enough to be attributed to preferential evaporation. In this zone, preferential evaporation cannot be clearly distinguished from experiment uncertainties.

- Outside these limits, variations of ratio are significant compared to the measurement accuracy and uncertainty showing that preferential evaporation effects are significant.

FIG3

Figure 3: Average signal ratio image calculated from the images obtained in configuration B (Iso-filter), at 573K. Color scale indicates the magnitude of the ratio.

FIG4

Figure 4: Measurement uncertainity obtained in configuration B (Iso-filter), at 573K. Color scale indicates the uncertainity.

For the different configuration under investigation (Table 1~~Table 1~~), the iso-filter image obtained in configuration B were recorded and analyzed. In all configuration tested, similar standard deviations and thus measurement uncertainty are obtained, with values close to 0.06. This result shows that the systematic error is 0.06 for all conditions investigated.

b. Reference configuration

Once the accuracy and measurement uncertainty of the methodology have been determined, a quantitative analysis of the results obtained in configuration A (i.e. with different filter on each channel) can be performed. Figure 5~~Figure 4~~ presents the average ratio of fluorescence signal for the surrogate fuel at 573K (Pinj=200bar). The magnitude of the variation of ratio is high (the standard deviation of this image is equal to 0.16), and the comparison with the measurement uncertainty image of Figure 4 shows that it is significantly higher that the measurement uncertainty determined in the previous section (in particular considering the central portions of the plumes), showing that preferential evaporation effects are significant in this condition.

The image of figure 3 shows that, unlike the image obtained in configuration B where a spatially homogeneous ratio map is observed, significant deviation from unity are observed in well-defined areas of the spray. A zone of ratio lower than unity (low volatility) is observed at the tail of the plumes while ratio higher than unity (high volatility) are observed at the tip. This result clearly indicates that preferential evaporation is significant in this condition, resulting in significant composition heterogeneities. The relative localization of low and high volatility components will be discussed in section 4.a. It is interesting to note that these results are similar to the ones obtained by Itani et al.[17,12] in different conditions..

Instantaneous images obtained in these conditions are presented in Figure 6~~Figure 5~~. The individual images differ from the average by the corrugated shape of the plumes, which is consistent with the turbulent nature of the mixing process. However the global low/high volatility tracer distribution is unchanged, showing that the average picture is representative of the individual events. This observation holds for all conditions investigated. Therefore only average results will be reported in the rest of this paper.

FIG5

Figure 5: Average ratio image of fluorescence signal for surrogate fuel (Pinj=200bar) at 573K. Mean ratio in the spray region is equal to 0.99, and the standard deviation is 0.16.

FIG6a&b

Figure 6: Exemple of instantaneous fluorescence ratio obtained for surrogate at 573K (200bar). The color scale on the right hand side indicates the magnitude of the ratio.

c. Effect of ethanol addition

Figure 7~~Figure 6~~ shows the average fluorescence ratio obtained with E20 and E85, in comparison with the surrogate fuel. Globally a similar result is obtained for E20 compared to the surrogate fuel only. The standard deviation of the average fluorescence signal is equal to 0.17 which is slightly higher than the surrogate fuel only. This seems to indicate that preferential evaporation is globally increasing with ethanol addition, but the difference is not enough to be significant. In general the distribution of the image is similar, with low volatility zone at the tail and high volatility zones at the tip. The extent

of low and high volatility zones regarding to the area where the ratio is close to unity is slightly increasing compared to the surrogate fuel only condition, further confirming the trend of enhanced preferential evaporation effect.

FIG 7a&b&c

Figure 7: Average fluorescence ratio at 573K (Pinj=200bar) for surrogate (left, Mean=0.99, Std=0.16), E20 (middle, Mean=1.00, Std=0.17) and E85 (right, Mean=1.03, Std=0.29) fuels. The color scale on the right hand side indicates the magnitude of the ratio.

The right side of Figure 7~~Figure 6~~ shows the average ratio image obtained in configuration A for the E85 fuel. The histogram of the fluorescence signal ratio, presented in Figure 8~~Figure 7~~, clearly features a bimodal shape with a very high standard deviation (0.29). Also, it can be observed that the global shape of the spray is modified: the spray plumes are thinner than for previous cases. The tracer zone corresponding to low volatility components extends over a much larger surface at the tail, with low value of the ratio (around 0.6 and up to 0.4). At the tip of each plume, an arrow shape is formed with high volatility components surrounding the whole tip. The ratio values obtained in this zone can be very high (from 1.3 until 1.6), well above the measurement uncertainty (Figure 4). These results indicate that preferential evaporation effects are significantly increased in this configuration where a significant amount of ethanol is added in the mixture.

Fig 8

Figure 8: Histogram of fluorescence ratio from average images, for different fuels at 573K, 200bar of injection pressure.

d. Effect of ambient temperature

The effect of ambient temperature on preferential evaporation is investigated here. Identical variations of ambient temperature have been carried on for the different fuels (surrogate, E20 and E85). However only the results obtained with E20 will be reported here because of the high level of similarity with others fuels.

Figure 9~~Figure 8~~ shows the average ratio of fluorescence signal for E20 at an ambient temperature of 525K (50K lower than the reference condition). Preferential evaporation is clearly visible. The standard deviation of the different filter images is equal to 0.2, while it was 0.17 at 573K, showing that the magnitude of preferential evaporation increases when temperature is reduced. As seen in the histogram (Figure 10~~Figure 9~~), the ratio distribution is obviously bimodal. The first mode is at a ratio=0.75 and stands for the low volatility tracer. The second mode corresponds to a ratio around 1.1-1.15 and it represents the high volatility tracer. Globally, the distribution of the low and high volatility region is similar, the only difference being the magnitude of the effect.

Fig 9 a&b&c

Figure 9: Average fluorescence ratio map for different ambient temperature in the Vessel with E20 fuel. From left to right: 525K (Mean=1.01, Std=0.20), 573K (Mean=1.00, Std=0.17) and 625K (Mean=0.99, Std=0.15). The color scale on the right hand side indicates the magnitude of the ratio.

At 625k, the distribution of ratio does not seem to be affected but a slight reduction of the variation of ratio is observed, which is consistent with the lower standard deviation of 0.15 obtained in this condition, which is lower than for the reference ambient temperature. This result tends to confirm that preferential evaporation effect is reduced when the temperature is increased. This observation is coherent with the faster evaporation. Thus, a higher amount of high and low volatility component evaporate simultaneously and induce lower component segregation.

Fig 10

Figure 10: Histogram of fluorescence ratio for different ambient temperature, for E20 fuel.

e. Effect of Injection pressure

In this section, the results obtained with a lower injection pressure are presented. Similarly to the other conditions, preliminary Mie scattering visualization were performed to verify that liquid droplets are fully evaporated at the time of imaging. It showed that at the injection pressure of 100bar, liquid droplets are still present in the area of visualization at the visualization time. Since the 2 tracer LIF technique is only valid in the fully vaporized region, this lower injection condition investigation was carried out at higher temperature, 625K, since the Mie Scattering visualization showed that the droplet are fully evaporated at this higher temperature. Therefore, the comparison with the higher injection pressure (200bar) condition is also carried out at this higher temperature to isolate the effect of injection pressure.

Figure 11~~Figure 10~~ shows the tracer ratio maps obtained for these two conditions of reference injection pressure (200bar) and lower injection pressure (100bar) respectively. The difference between the two images, in terms of ratio distribution or standard deviation are not straightforward. The same ratio distribution is observed in both cases, with the low volatility tracer at the tail and the high volatility at the tip. To deepen the analysis, histograms of the ratio distribution in the images is displayed in figure 11. The difference within the two cases appears more clearly in the histograms. The lower injection pressure conditions dispays a bimodal distribution while it is not the case for the high injection pressure condition, indicating that the former is slightly more heterogeneous than the latter. This observation is coherent with the fact that injection pressure enhances the atomization process[27]. Indeed, it is probable that the atomization process is reduced at lower pressure, resulting in bigger droplet sizes hence in slower evaporation, enhancing preferential evaporation effect. This slower evaporation for lower injection pressure is in addition confirmed by the Mie Scattering visualization that shows the presence of droplet at the image timing when the ambient temperature is 573K.

Fig 11 a&b

Figure 11: Ratio of fluorescence signal for the surrogate fuel at 625K, Pinj=200bar (Top, Mean=0.99, Std=0.13) and Pinj=100bar(Bottom, Mean=0.99, Std=0.13). The color scale on the right hand side indicates the magnitude of the ratio.

Fig 12

Figure 12: Histogram of fluorescence ratio for surrogate fuel at different injection pressure (625K).

4. Discussion

In the previous section we have shown that the measurement of the relative distributions of high and low volatility tracers clearly indicates the presence of preferential evaporation effects on the tracer distribution in the operating conditions investigated. A high volatility tracer zone is observed at the tip of the spray while a low volatility tracer zone is observed at the tail, in the central zone. In this section we will discuss the processes at the origin of this distribution. Also while the measurement gives information on the tracer distribution, a deeper analysis can be performed using the thermodynamic model to relate the tracer distribution with that of the fuel components. For this purpose, the composition maps described in [20] will be used here to derive information on the fuel component distribution from the ratio measurements. In particular it will be interesting to analyze if the effect of ethanol addition on the ratio images observed in the previous section also correspond to an increased segregation of the fuel components as an effect of preferential evaporation. Finally the effect of the thermodynamic model uncertainties on the analysis will be discussed.

a. Analysis of the aerodynamic mechanism leading to the component distribution

It has been shown previously that for the reference configuration, a significant preferential evaporation effect is observed. However, the spatial segregation of the different components (low/high volatility) is not so straightforward to understand and requires an deeper analysis. Indeed an intuitive first level interpretation based on the idea that droplets with higher inertia travel farther downstream of the spray than the evaporated fuel would lead to an opposite distribution of low and high volatility components since these evaporating droplets would transport the heavy components at the tip of the plumes. We will see in the following that this analysis very probably fails in the present case.

The Spray G injector is a multi-hole injector that produces a full-cone spray. The injection pressure is the main driver that initially pushes the spray inside the chamber allowing for the liquid spray to penetrate at early injection timings. Previous analysis of the mixture formation process in the spray G conditions[28–30] have shown that during injection, a strong aerodynamic motion is generated by air entrainment which persists

after the end of injection. This motion becomes the main driver for the propagation of the vaporized fuel jet[30]. Since the high-volatility components evaporate more rapidly than the low-volatility components, the mechanism more likely to occur is that the former are vaporized and preferentially entrained by the aerodynamic motion at a time when the low-volatility components are still liquid. As a result, the high-volatility components are entrained at the tip of the jet while the low-volatility components remain in the upper part of the jet, as it can be seen in Figure 5~~Figure 4~~. With such a mechanism in mind, the effect of parameter variation becomes more obvious. Ambient temperature increase accelerates the evaporation by reducing the droplet lifetime[6] therefore reducing the amount of high volatility components entrained at the tip relative to low volatility components. Similarly, reducing the injection pressure tends to increase droplet diameter[27] and therefore to slow down the evaporation process, decreasing the amount of light components entrained at the tip of the plumes by the aerodynamic motion.

b. Relation between tracer and fuel component segregation

The results presented so far has demonstrated that the effect of sequential evaporation is significant and results in spatial distribution heterogeneities between the high and low volatility tracers. Also it was found that variations of ambient conditions such as ambient temperature, injection pressure or fuel composition affects this phenomena. However, since these variations also affect the way the fluorescent tracers evaporate relative to the fuel component, it is not straightforward to analyze the effects of these variations on the local fuel component distribution.

In order to obtain this kind of information, the thermodynamic model was used here to relate the fuel tracer ratio maps to the fuel component distributions. In particular, the fuel composition maps obtained in [20] were used to derive spatial component distribution maps from the tracer ratio images obtained by 2C LIF. Figure 13~~Figure 12~~ presents the result of this combination. The images display the proportion of the two high volatility components (n-pentane, iso-octane) in the mixture in the top row and that of the low volatility (n undecane) one in the bottom row, calculated according to the following equations:

$$High\ Volatility = \frac{m_{n-pentane} + m_{iso-octane}}{m_{n-pentane} + m_{iso-octane} + m_{undecane}}$$

$$Low\ Volatility = \frac{m_{undecane}}{m_{n-pentane} + m_{iso-octane} + m_{undecane}}$$

. Only the left hand side image corresponding to the surrogate fuel is commented in this section, the two right hand side images corresponding to the mixture of surrogate and ethanol will be commented in the next section. This image corresponding to the surrogate fuel condition presents the same segregation than the fluorescence ratio maps displayed before. The high volatility components proportion varies between more than

80% at the plumes tip and less than 70% at the plumes tail, and inversely for the low volatility component. This result therefore shows that the sequential evaporation effect results in segregation of fuel component in the vapor plumes. This segregation, if it persist in the combustion chamber after mixing of the plumes with the ambient air through turbulent mixing, might result in variation of the flame propagation speed or in variation of the auto-ignition properties, therefore affecting the knocking behavior of the engine.

Fig13

Figure 13: high (n-pentane, iso-octane, top row) and low (n undecane, bottom row) volatility spatial distribution for the different fuel used at 200bar of injection pressure and 573K of ambient temperature. From left to right: surrogate, E20 and E85. The color scale on the right hand side indicates the magnitude of the ratio.

c. Effect of ethanol addition on the fuel component distribution

As presented in the previous sections, ethanol addition strongly affects the evaporation process and the spatial segregation of the high and low volatility tracers. But again the analysis of this effect on the fuel component distribution requires the use of the thermodynamic model to relate tracer ratio maps with the fuel component distribution. The right hand side images of Figure 13~~Figure 12~~ displays the result of this analysis for E20 and E85 fuel mixtures.

This figure clearly shows that ethanol addition enhances low and high volatility component segregation. Compared to the surrogate fuel, the amplitude of high volatility proportion variation increases, and in particular the proportion of the low volatility proportion in the tail reduces progressively from approximately more than 70% for the surrogate to less than 65% for E85. This result shows that ethanol addition affects the relative evaporation of iso-octane, pentane and undecane, and is consistent with the azeotropic behavior of ethanol when mixed with iso-octane or pentane[5,7,8].

d. Measurement uncertainties related to the thermodynamic model

In addition to the measurement uncertainties related to the measurement of the tracers' ratio, the transcription of this information into fuel composition maps is subject to additional uncertainties related on one part to the simplifying hypothesis required to relate the thermodynamic model to the spray images, and on the other part on the uncertainties related to the thermodynamical model itself. The determination of the former uncertainties requires a detailed investigation of the validity of the hypothesis made to apply the thermodynamical model to the spray evaporation. Unfortunately this is beyond the scope of this work and it will have to be taken into account in future analysis. The uncertainties related to the thermodynamical model itself have been the scope of the

work presented in [20]. The latter showed that for E00 and E20 the uncertainties related to the thermodynamic model are below 5% and therefore can be neglected. However, the analysis showed that for E85 the measurement uncertainty related to the model are higher. Fortunately, the results of Figure 14 show that the observed effect are very significant, so that although the use of these results for a quantitative analysis will have to take into account the associated measurement uncertainty, the latter is not affecting the qualitative observations made during the present work.

5. Conclusions

A 2 tracers LIF measurement technique was developed and applied to investigate the effect of preferential evaporation on the mixture composition of gasoline spray in a high pressure high temperature vessel. It was then coupled to a thermodynamic model to derive information on fuel component distribution. The experimental conditions correspond to the ECN Spray G target. A surrogate fuel was designed using the thermodynamic model to well represent the commercial gasoline evaporation characteristics while being transparent to laser excitation in order to enable the use of fluorescent tracers. The effect of ethanol addition was investigated by performing experiments with two additional fuels: E20 and E85. The uncertainty of the measurement technique was determined though a dedicated methodology to enable quantitative measurements. Also, a thermodynamic model was used to relate the tracer' ratio map to fuel composition maps. A significant preferential evaporation effect was observed in these conditions representative of engine applications. It was found that the air entrainment dynamic generated during injection entrains the high volatility components to the tip of the spray while the low volatility components remain in the tail. Finally it was found that the addition of ethanol enhances the preferential evaporation effect resulting in a significant increase of the segregation between high and low volatility components after evaporation. The obtained results highlight the potential of this two tracers LIF measurement technique to provide understanding on the evaporation process of multicomponent fuels, which is of particular interest for the validation of numerical models.

Various perspectives of this work can be draw, such as the application of this technique to more and more complex conditions, i.e. in presence of oxygen and/or with a more representative surrogate fuel (not only for evaporation but also for viscosity, density, burning velocity…). Also, other engine application can be considered, like characterization of mixture formation in multicomponent spray/wall interactions.

Acknowledgements

FVV funding is greatly acknowledged (agreement 6011101, Bioptic2 project). Also the technical expertise of Clément Bramoulle is greatly acknowledged.

References

1. Baumgarten C. *Mixture formation in internal combustion engines*. Berlin: Springer, 2006.
2. Bandel W, Fraidl GK, Kapus PE, Sikinger H and Cowland CN. The Turbocharged GDI Engine: Boosted Synergies for High Fuel Economy Plus Ultra-low Emission. In: *SAE 2006 World Congress & Exhibition,* APR. 03, 2006: SAE International400 Commonwealth Drive, Warrendale, PA, United States.
3. Joshi, S., Lave, L., Maclean, H. and Lankey, R. A Life Cycle Comparison of Alternative Transportation Fuels. *SAE Int. J. Engines* 2000.
4. Zhang B and Sarathy SM. Lifecycle optimized ethanol-gasoline blends for turbocharged engines. *Applied Energy* 2016; 181: 38–53.
5. Bader A, Keller P and Hasse C. The influence of non-ideal vapor–liquid equilibrium on the evaporation of ethanol/iso-octane droplets. *International Journal of Heat and Mass Transfer* 2013; 64: 547–558.
6. Keller P, Knorsch T, Wensing M and Hasse C. Experimental and numerical analysis of iso-octane/ethanol sprays under gasoline engine conditions. *International Journal of Heat and Mass Transfer* 2015; 84: 497–510.
7. Lide DR and Kehiaian HV. *CRC handbook of thermophysical and thermochemical data*. Boca Raton: CRC Press, 1994.
8. Horsley LH and Tamplin WS. *Azeotropic data*. Washington: American Chemical Society, 1952-73.

9. Whitaker, P., Shen, Y., Spanner, C., Fuchs, H., Agarwal, A., Byrd, K. Development of the Combustion System for a Flexible Fuel Turbocharged Direct Injection Engine. *SAE Int. J. Engines* 2010.
10. Marriott, C.D., Wiles, M.A., GwidtShibata, J.M. and Parrish, S.E. Development of a Naturally Aspirated Spark Ignition Direct-Injection Flex-Fuel Engine. *SAE Int. J. Engines* 2008.
11. Itani Lama M., Bruneaux G, Hermant L and Schulz C. Investigation of the Mixing Process and the Fuel Mass Concentration Fields for a Gasoline Direct-Injection Spray at ECN Spray G Conditions and Variants: SAE International.
12. Itani LM, Bruneaux G, Di Lella A and Schulz C. Two-tracer LIF imaging of preferential evaporation of multi-component gasoline fuel sprays under engine conditions. *Proceedings of the Combustion Institute* 2015; 35: 2915–2922.
13. Schulz C and Sick V. Tracer-LIF diagnostics: quantitative measurement of fuel concentration, temperature and fuel/air ratio in practical combustion systems. *Progress in Energy and Combustion Science* 2005; 31: 75–121.
14. Ma X, He X, Wang J-x and Shuai S. Co-evaporative multi-component fuel design for in-cylinder PLIF measurement and application in gasoline direct injection research. *Applied Energy* 2011; 88: 2617–2627.
15. Kawanabe H, Tanaka S, Yamamoto S, Kojima H and Ishiyama T. PLIF Measurement of Fuel Concentration in a Diesel Spray of Two-component Fuel.
16. Einecke S, Schulz C and Sick V. Measurement of temperature, fuel concentration and equivalence ratio fields using tracer LIF in IC engine combustion. *Appl Phys B* 2000; 71: 717–723.
17. Itani L. Development and application of optical diagnostic techniques for assessing the effects of preferential evaporation of multi-component fuels under engine-relevant conditions. *PhD Thesis* 2015.

18. Krämer H, Einecke S, Schulz C, Sick V, Nattrass Steve R. and Kitching John S. Simultaneous Mapping of the Distribution of Different Fuel Volatility Classes Using Tracer-LIF Tomography in an IC Engine: SAE International.
19. Steeper R, De Zilwa Shane and Fayoux A. Co-Evaporative Tracer-PRF Mixtures For LIF Measurements in Optical HCCI Engines: SAE International.
20. Michele Bardi, Angela Di Lella, Gilles Bruneaux. Quantitative interpretation of two tracers laser induced fluorescence (2T-LIF) for preferential evaporation in GDI applications: technique definition and uncertainty assessment. *Fuel-submitted,* 2018.
21. Koban W, Schorr J and Schulz C. Oxygen-distribution imaging with a novel two-tracer laser-induced fluorescence technique. *Applied Physics B: Lasers and Optics* 2002; 74: 111–114.
22. Engine Combustion Network. *“Spray G Operating Condition”: Last update on December 03, 2014*, http://www.sandia.gov/ecn/G/targetCondition/sprayG.php.
23. Speight JG. *Synthetic fuels handbook: Properties, process, and performance*. New York: McGraw-Hill, 2008.
24. Faust S, Goschütz M, Kaiser SA, Dreier T and Schulz C. A comparison of selected organic tracers for quantitative scalar imaging in the gas phase via laser-induced fluorescence. *Appl. Phys. B* 2014; 117: 183–194.
25. Pickett LM, Genzale CL, Bruneaux G, et al. Comparison of Diesel Spray Combustion in Different High-Temperature, High-Pressure Facilities. *SAE Int. J. Engines* 2010; 3: 156–181.
26. Moffat RJ. Describing the uncertainties in experimental results. *Experimental Thermal and Fluid Science* 1988; 1: 3–17.
27. Lee S and Park S. Experimental study on spray break-up and atomization processes from GDI injector using high injection pressure up to 30MPa. *International Journal of Heat and Fluid Flow* 2014; 45: 14–22.

28. Sphicas P, Pickett LM, Skeen S, et al. A Comparison of Experimental and Modeled Velocity in Gasoline Direct-Injection Sprays with Plume Interaction and Collapse. *SAE Int. J. Fuels Lubr.* 2017; 10: 184–201.
29. Panos Sphicas, Lyle M. Pickett, Scott Skeen, Jonathan Frank, Tommaso Lucchini, David Sinoir, Gianluca D'Errico, Kaushik Saha, and Sibendu Som. Inter-plume aerodynamics for gasoline spray collapse. *IJER Accepted Paper*.
30. Fansler TD and Parrish SE. Spray measurement technology: a review. *Meas. Sci. Technol.* 2015; 26: 12002.

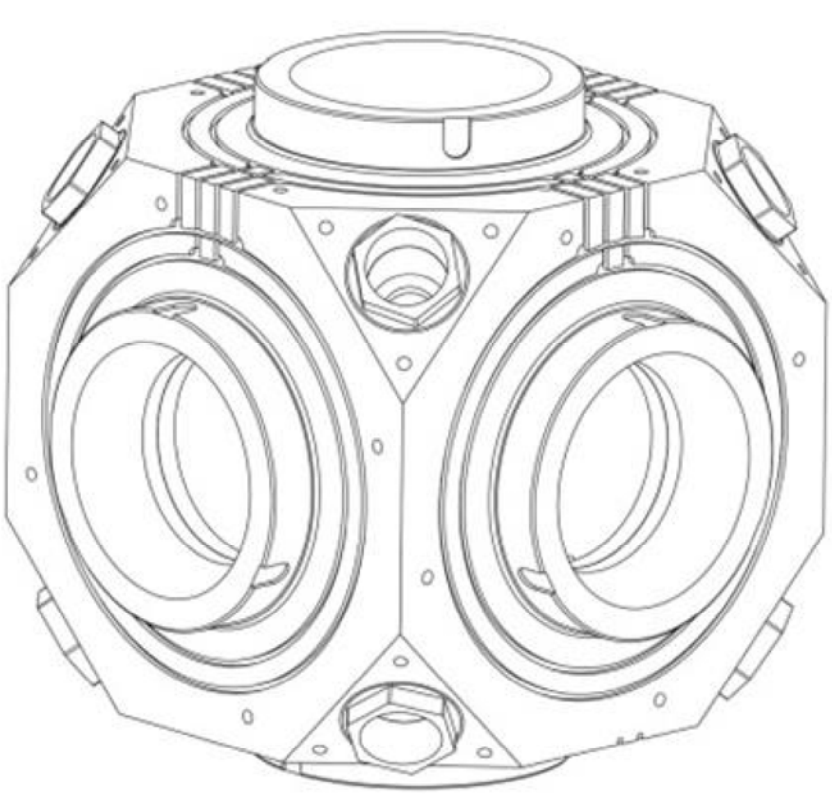

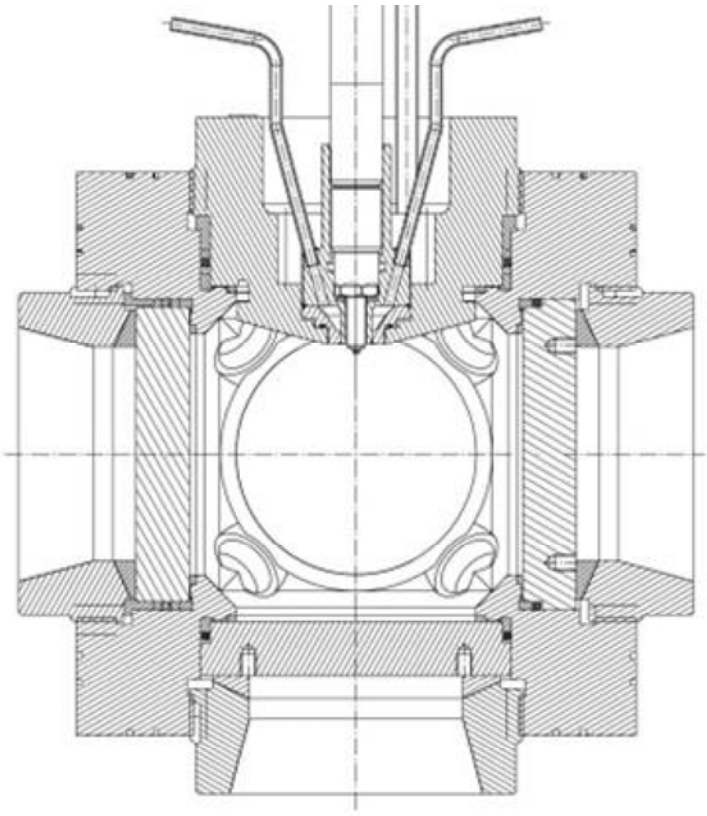

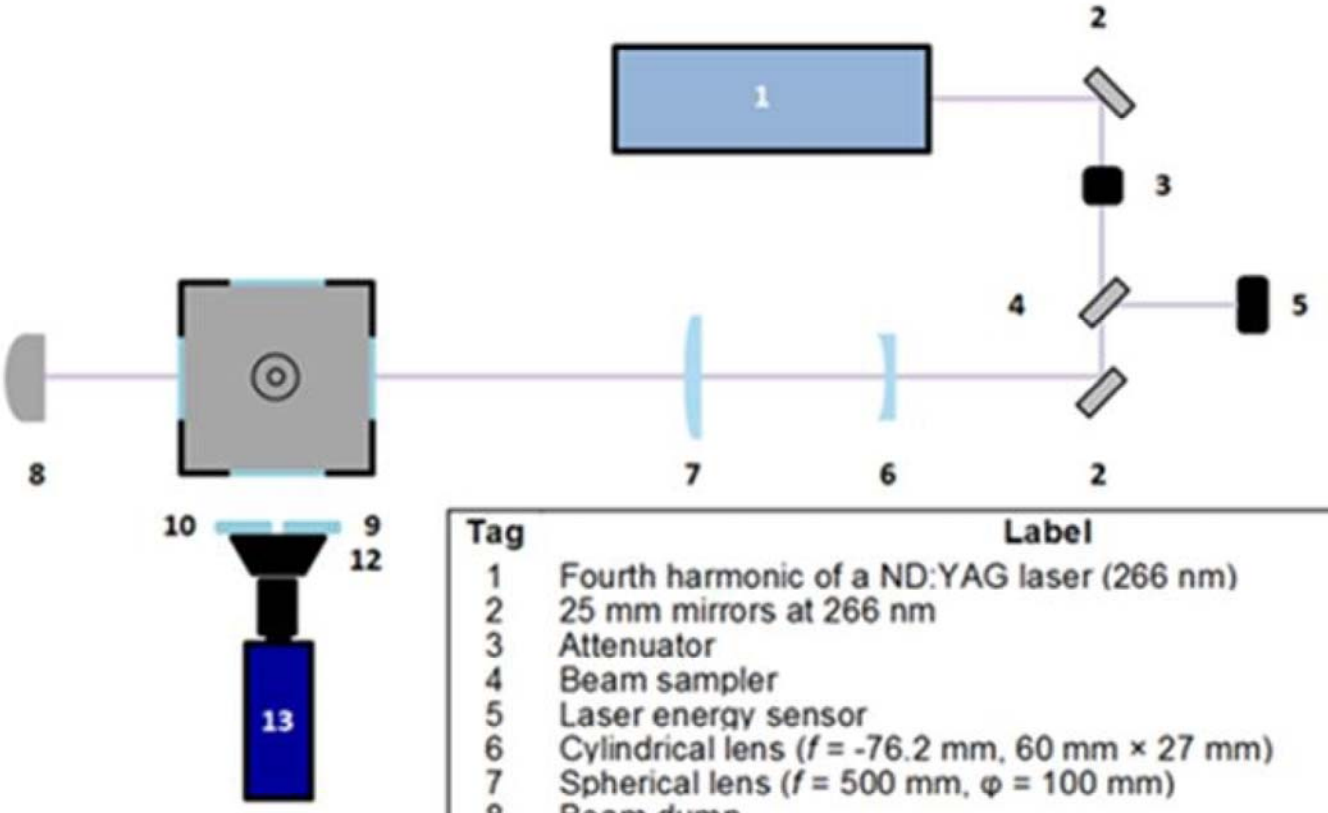

Tag	Label
1	Fourth harmonic of a ND:YAG laser (266 nm)
2	25 mm mirrors at 266 nm
3	Attenuator
4	Beam sampler
5	Laser energy sensor
6	Cylindrical lens (f = -76.2 mm, 60 mm × 27 mm)
7	Spherical lens (f = 500 mm, φ = 100 mm)
8	Beam dump
9	Band pass filter (Semrock, λ = 292±14 nm, transmissivity > 70%)
10	Band pass filter (Semrock, λ = 340±14 nm, transmissivity > 70%)
11	Band pass filter (Semrock, λ = 377±50 nm, transmissivity > 70%)
12	Image doubler
13	Camera 1

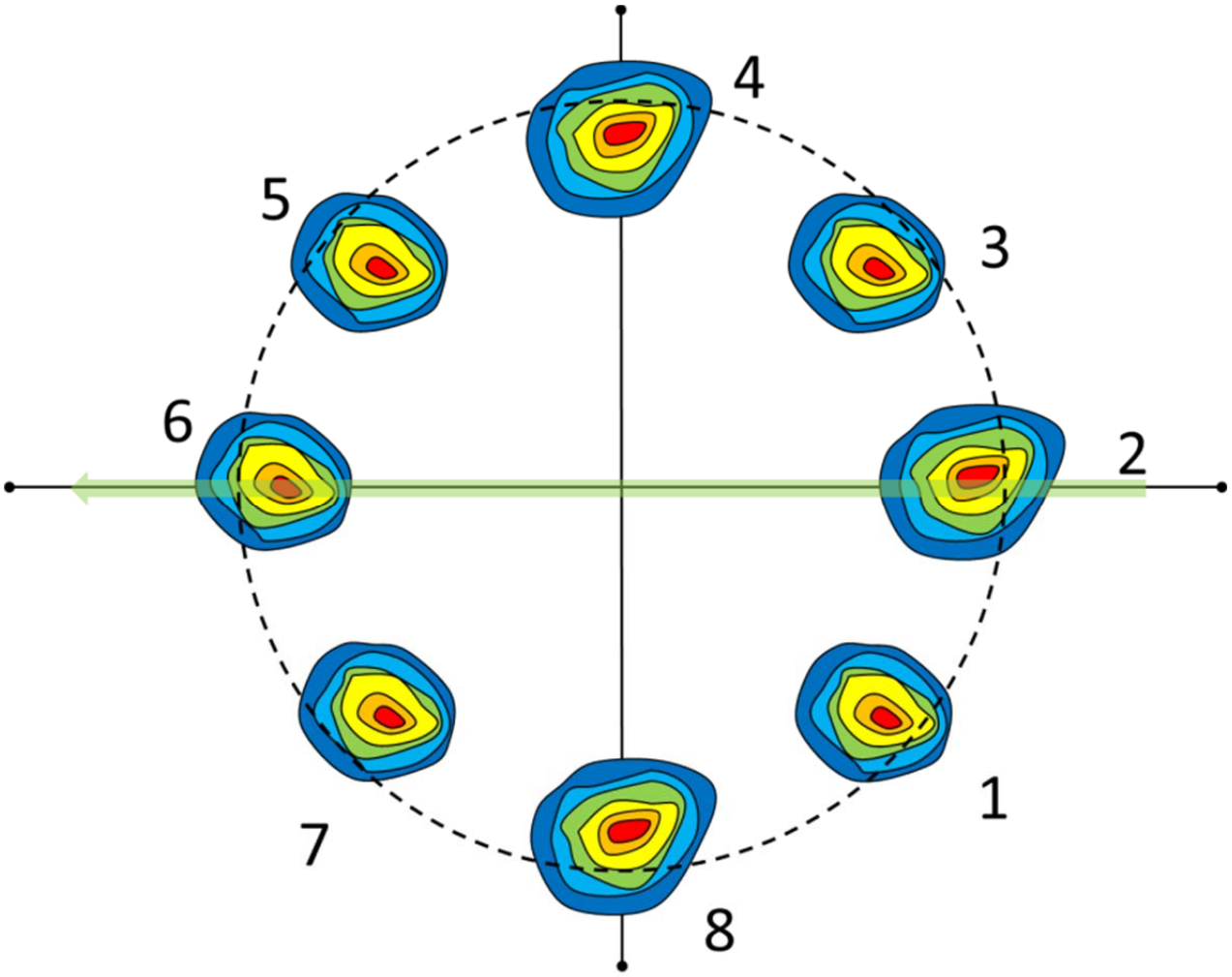
4
5
3
6
2
7
1
8

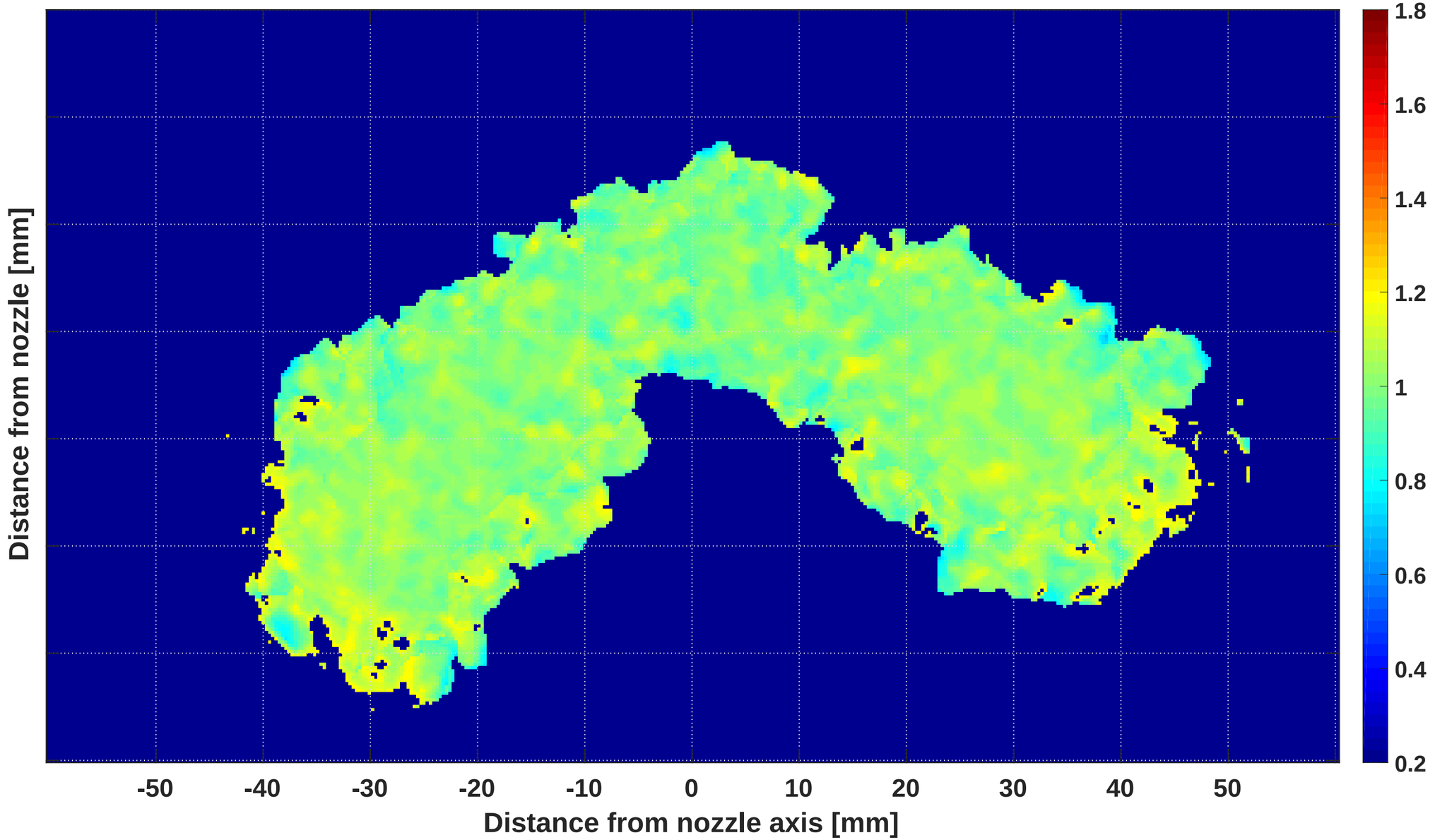
Distance from nozzle [mm]
-50
-40
-30
-20
-10
0
10
20
30
40
50
Distance from nozzle axis [mm]
1.8
1.6
1.4
1.2
1
0.8
0.6
0.4
0.2

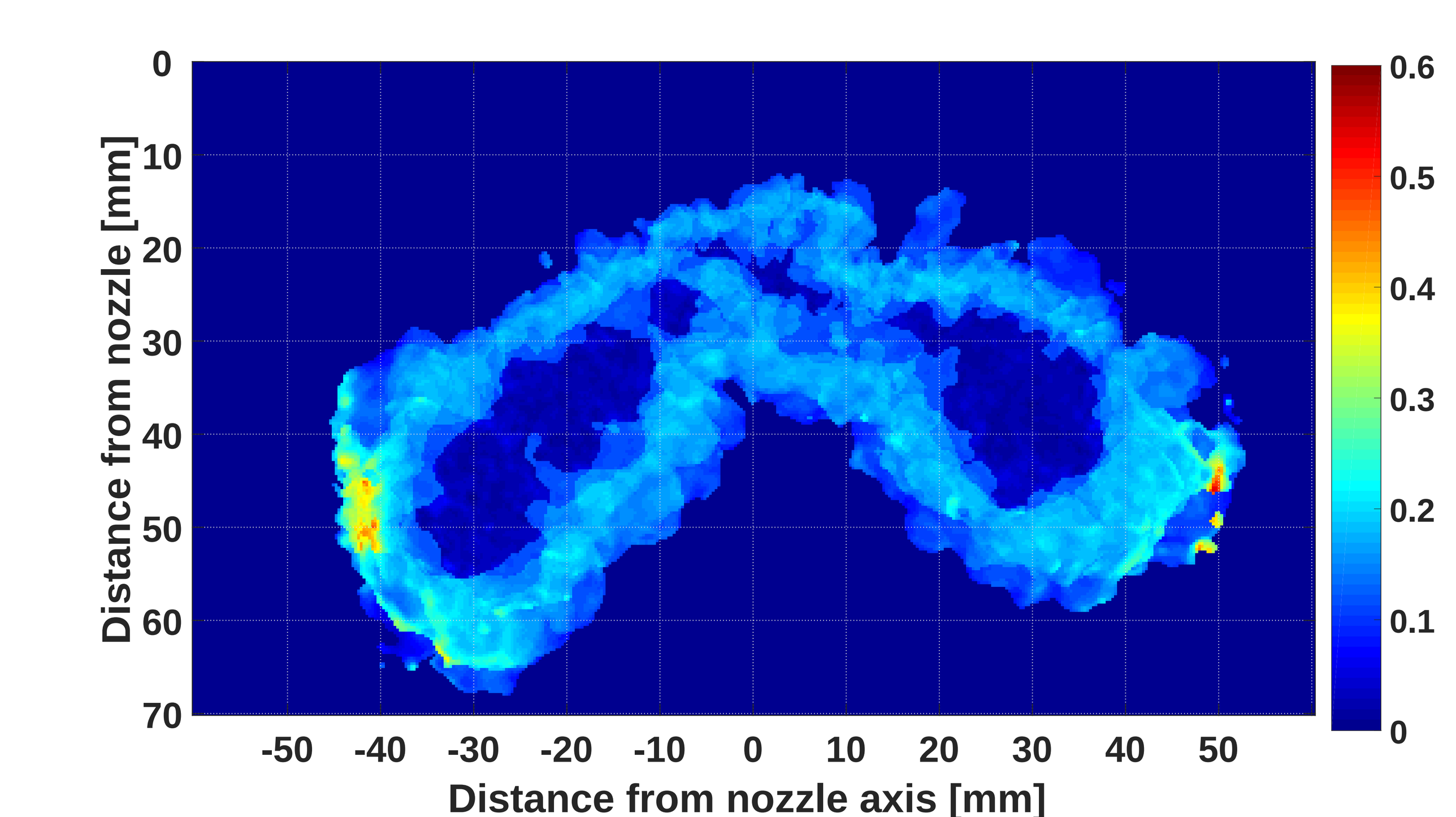
Distance from nozzle [mm]
0
10
20
30
40
50
60
70
-50
-40
-30
-20
-10
0
10
20
30
40
50
Distance from nozzle axis [mm]
0.6
0.5
0.4
0.3
0.2
0.1
0

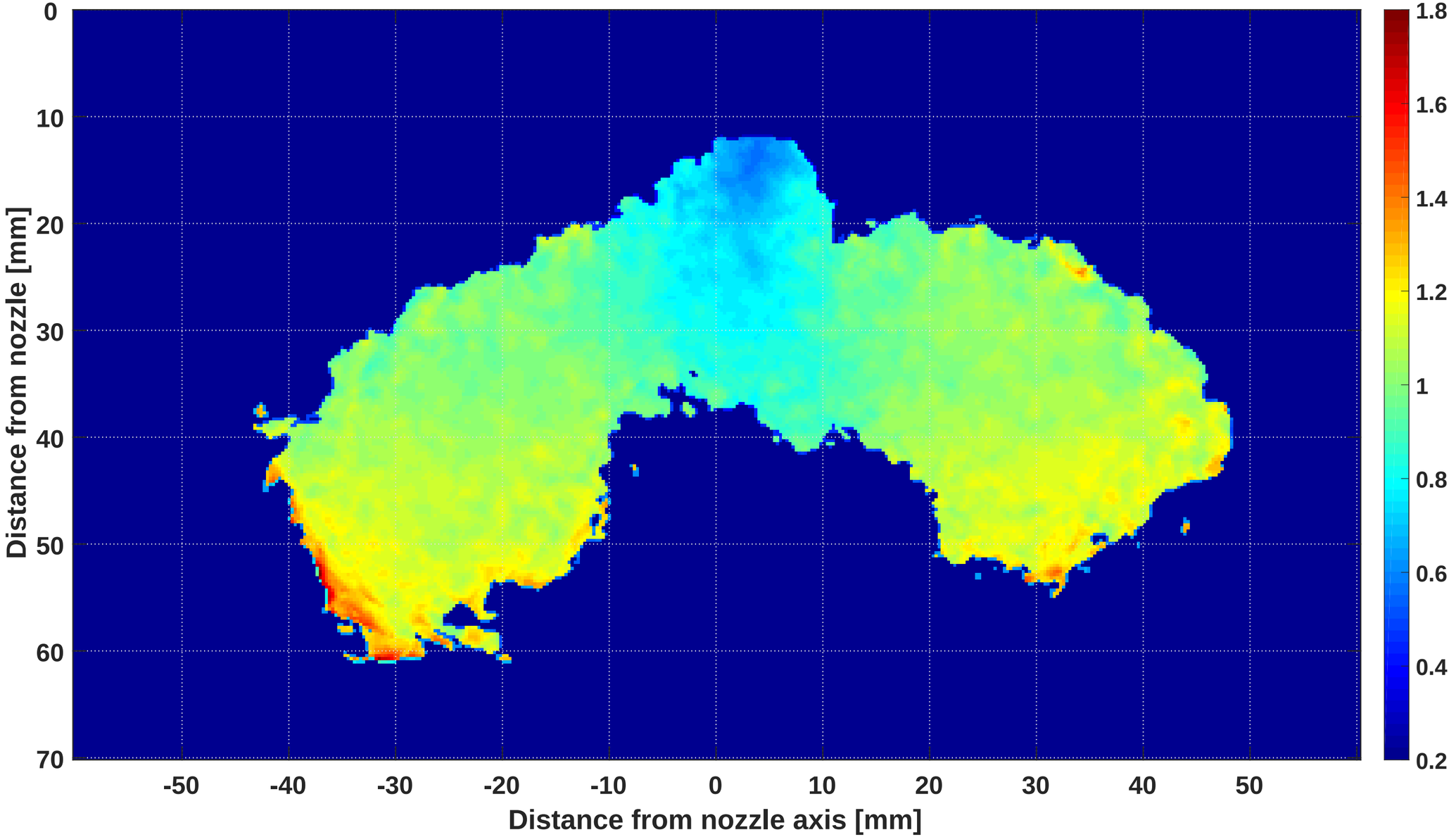
Distance from nozzle [mm]
0
10
20
30
40
50
60
70
-50
-40
-30
-20
-10
0
10
20
30
40
50
Distance from nozzle axis [mm]
1.8
1.6
1.4
1.2
1
0.8
0.6
0.4
0.2

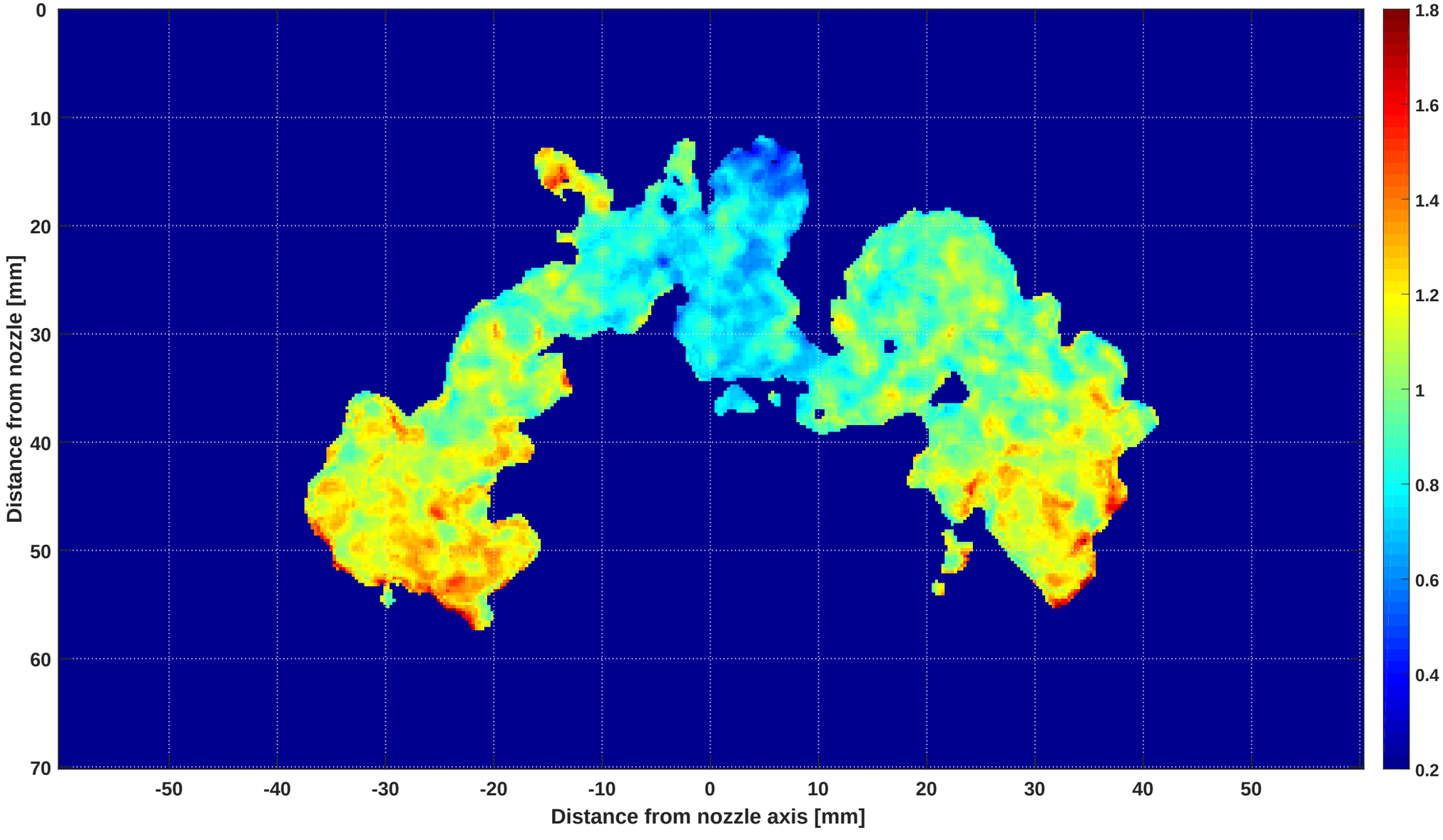
Distance from nozzle [mm]
0
10
20
30
40
50
60
70
-50
-40
-30
-20
-10
0
10
20
30
40
50
Distance from nozzle axis [mm]
1.8
1.6
1.4
1.2
1
0.8
0.6
0.4
0.2

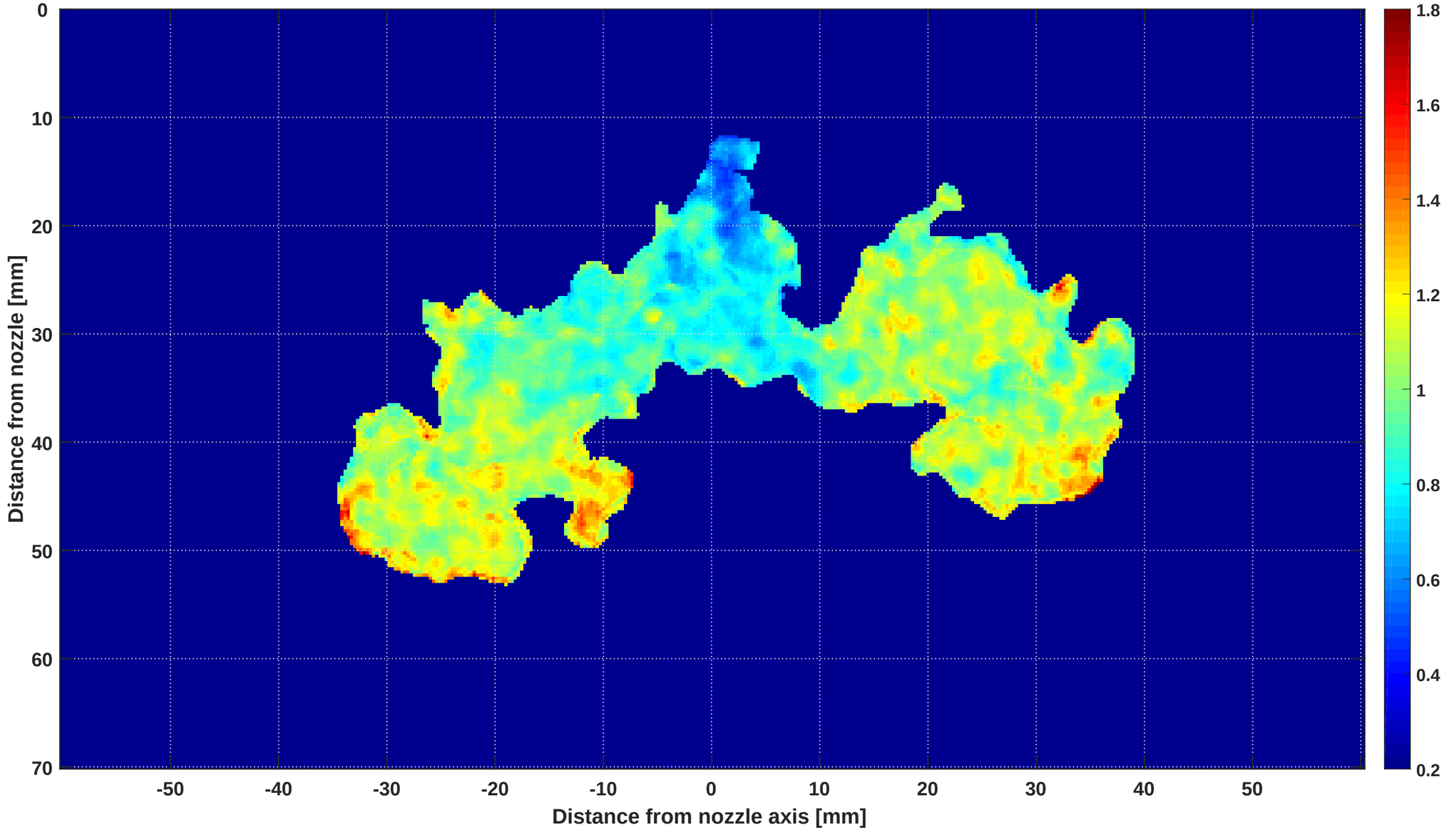
0
10
20
30
40
50
60
70
Distance from nozzle [mm]
-50
-40
-30
-20
-10
0
10
20
30
40
50
Distance from nozzle axis [mm]
1.8
1.6
1.4
1.2
1
0.8
0.6
0.4
0.2

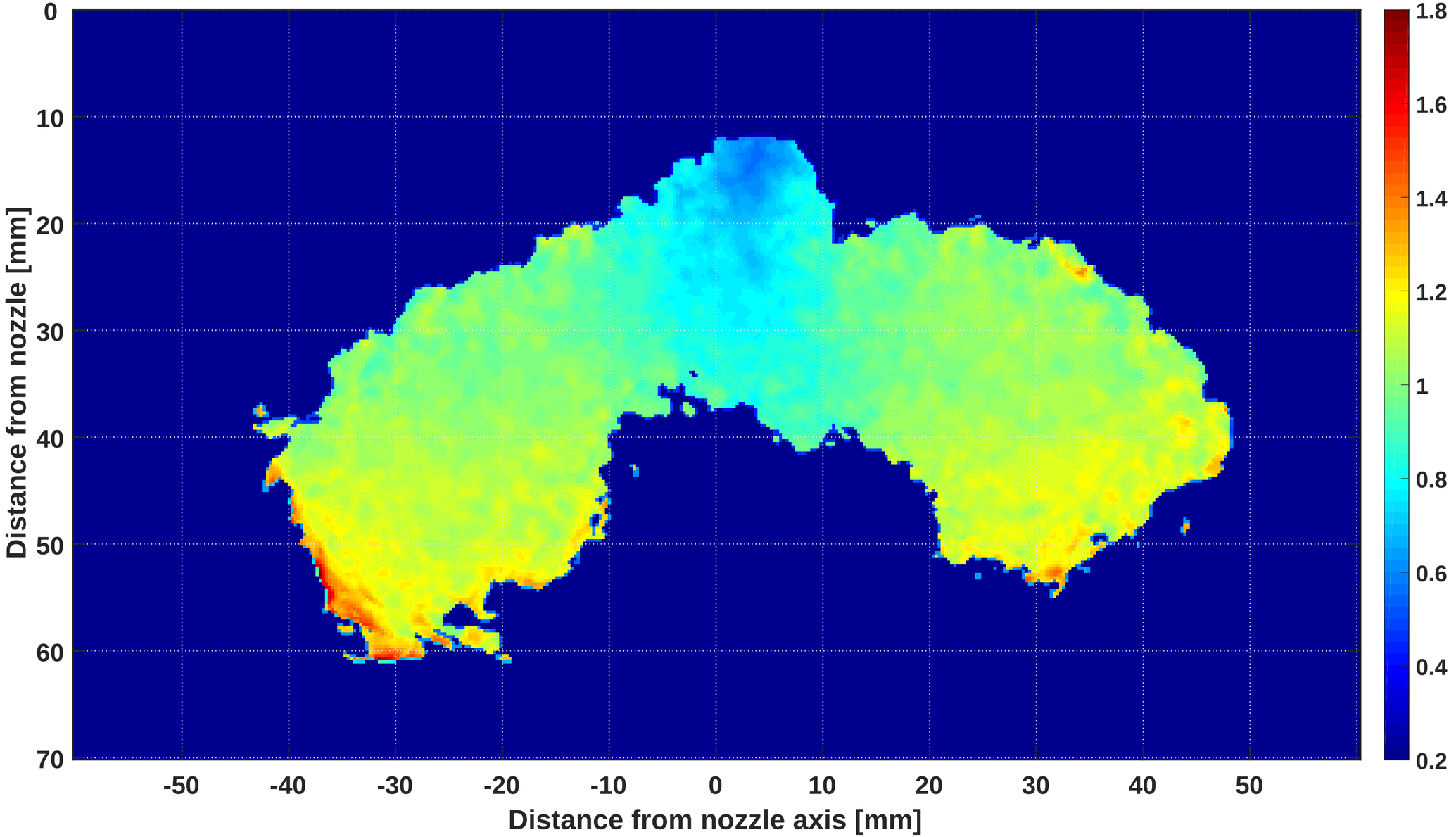
Distance from nozzle [mm]
0
10
20
30
40
50
60
70
-50
-40
-30
-20
-10
0
10
20
30
40
50
Distance from nozzle axis [mm]
1.8
1.6
1.4
1.2
1
0.8
0.6
0.4
0.2

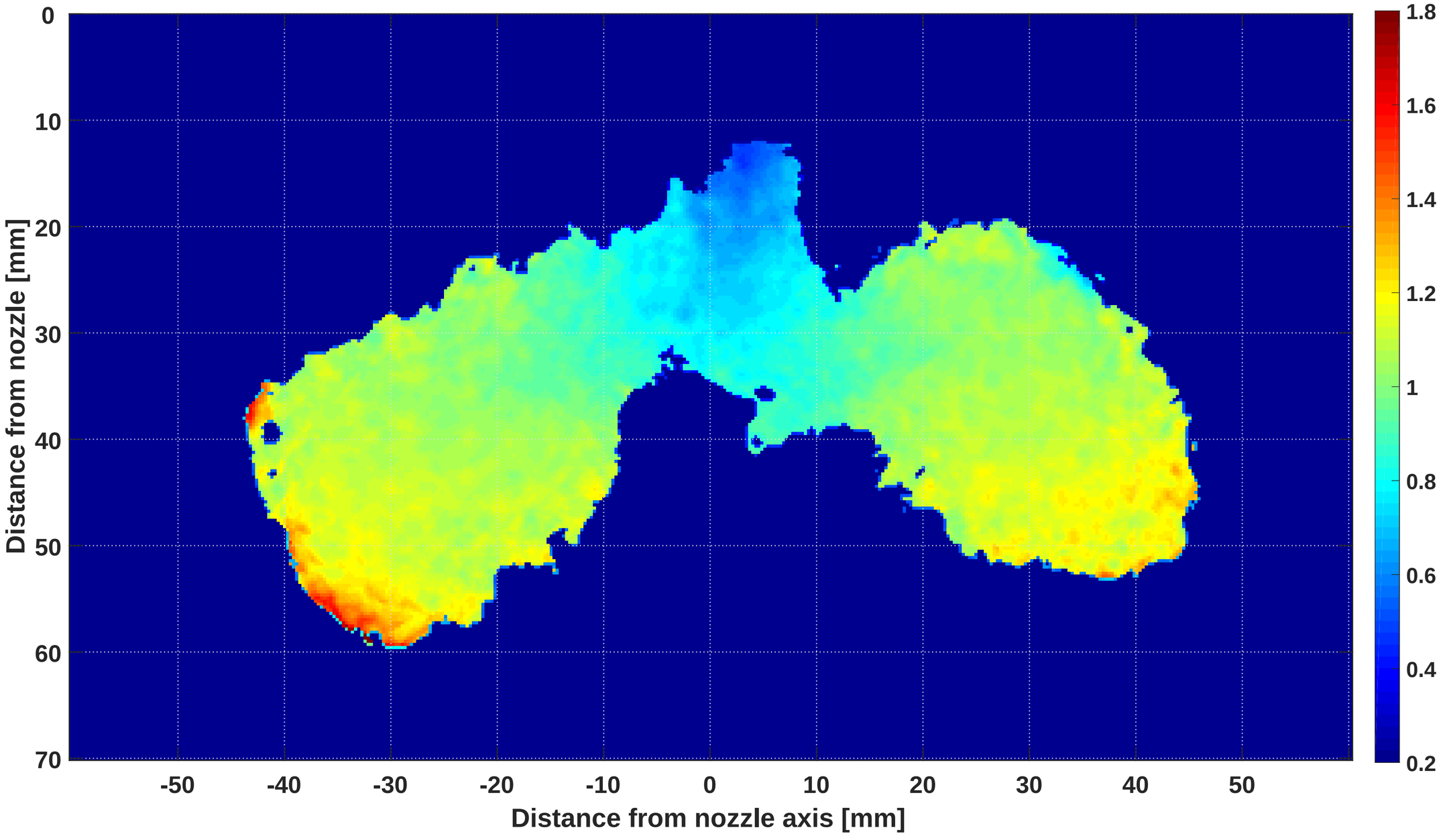
0
10
20
30
40
50
60
70
Distance from nozzle [mm]
-50
-40
-30
-20
-10
0
10
20
30
40
50
Distance from nozzle axis [mm]
1.8
1.6
1.4
1.2
1
0.8
0.6
0.4
0.2

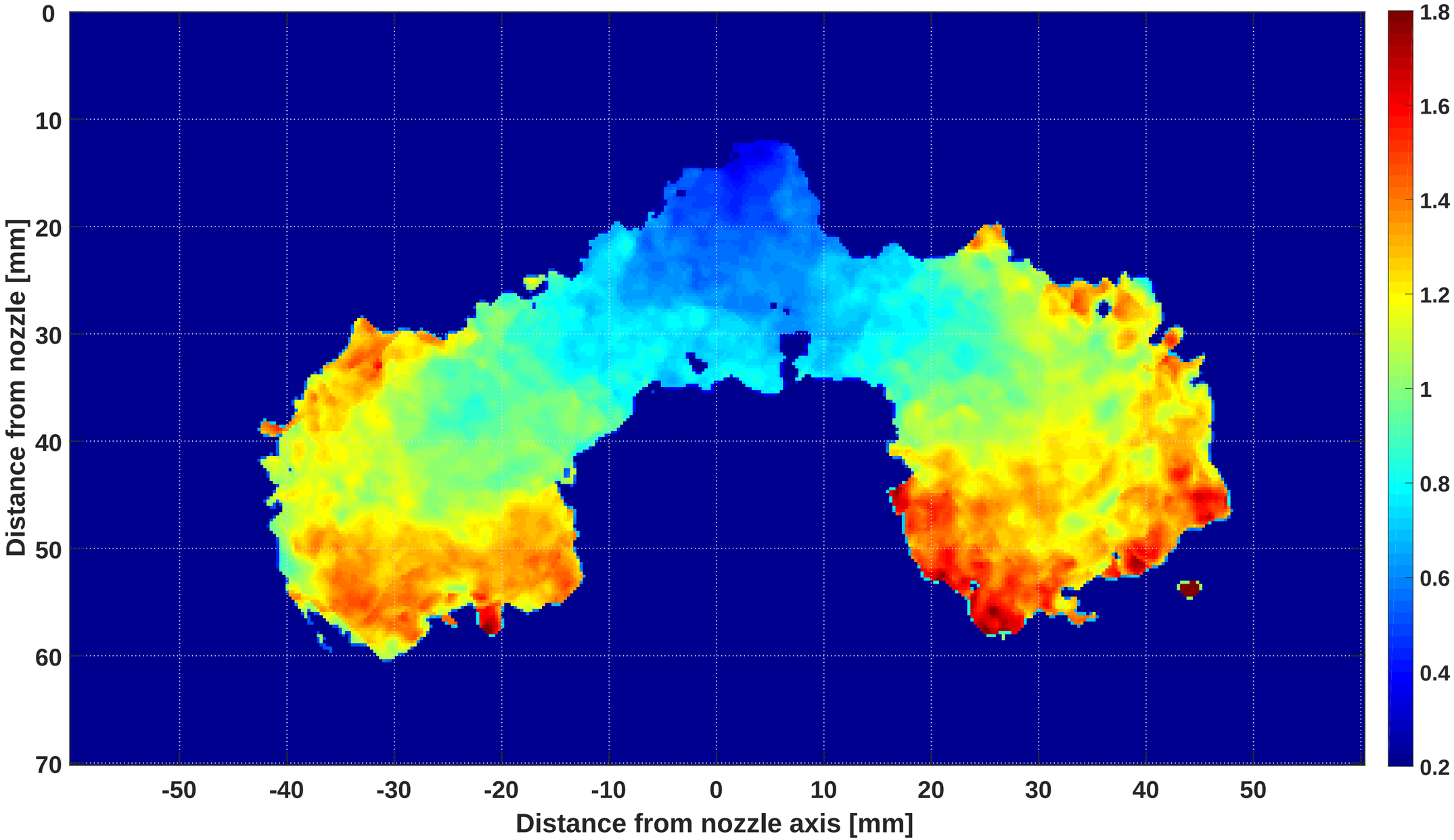
0
10
20
30
40
50
60
70
Distance from nozzle [mm]
-50
-40
-30
-20
-10
0
10
20
30
40
50
Distance from nozzle axis [mm]
1.8
1.6
1.4
1.2
1
0.8
0.6
0.4
0.2

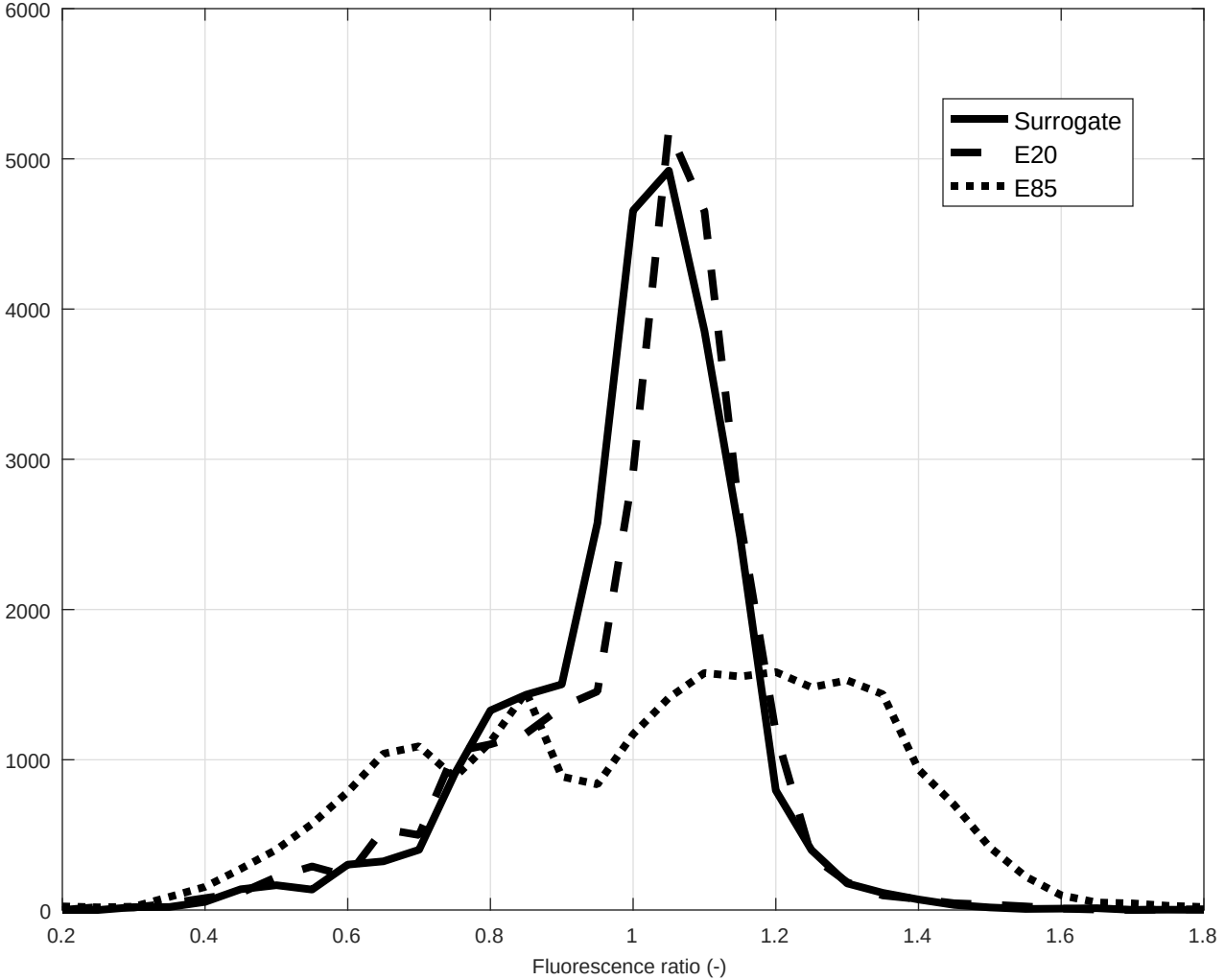
6000
5000
4000
3000
2000
1000
0
0.2
0.4
0.6
0.8
1
1.2
1.4
1.6
1.8
Fluorescence ratio (-)
Surrogate
E20
E85

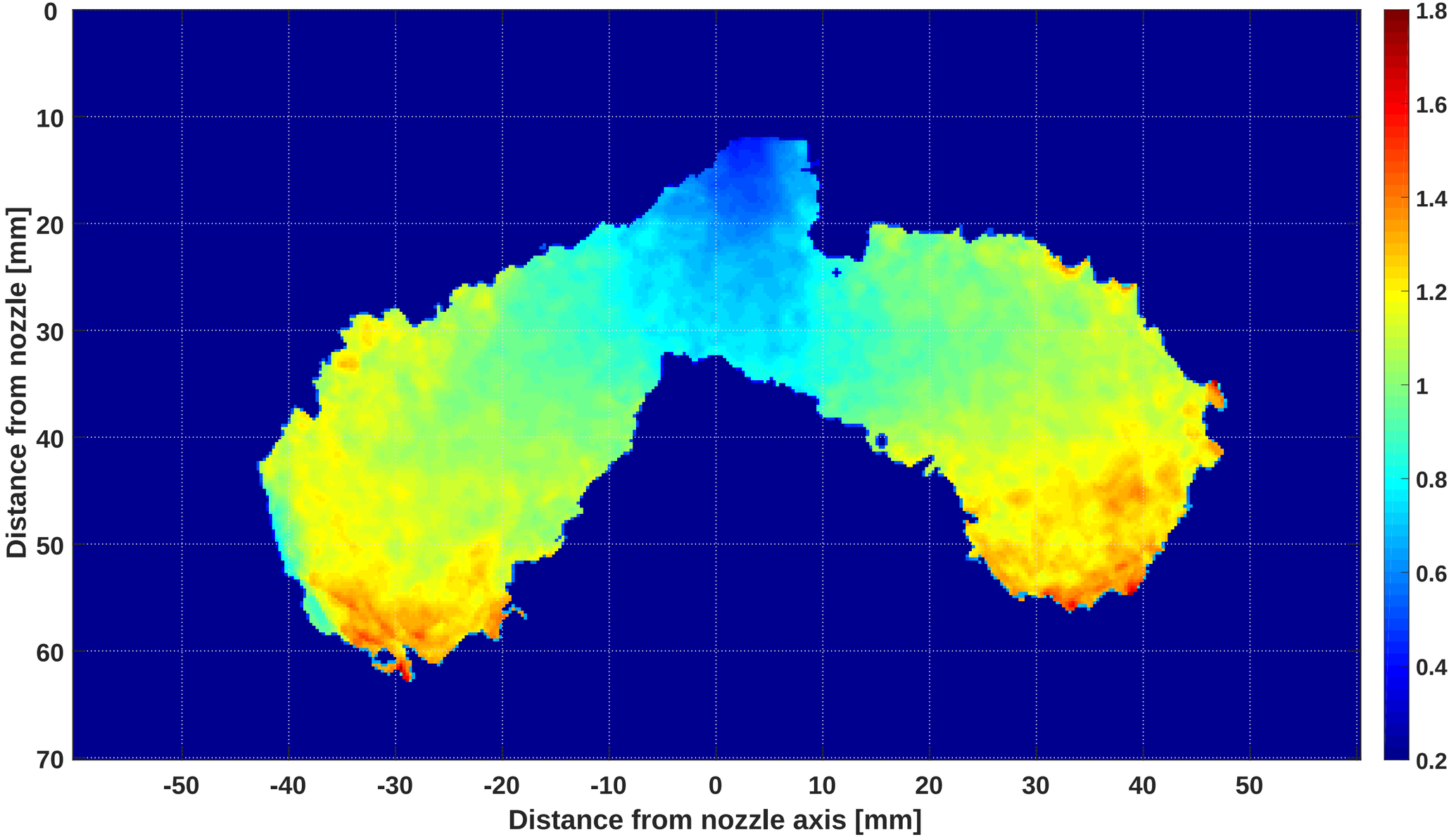
Distance from nozzle [mm]
0
10
20
30
40
50
60
70
-50
-40
-30
-20
-10
0
10
20
30
40
50
Distance from nozzle axis [mm]
1.8
1.6
1.4
1.2
1
0.8
0.6
0.4
0.2

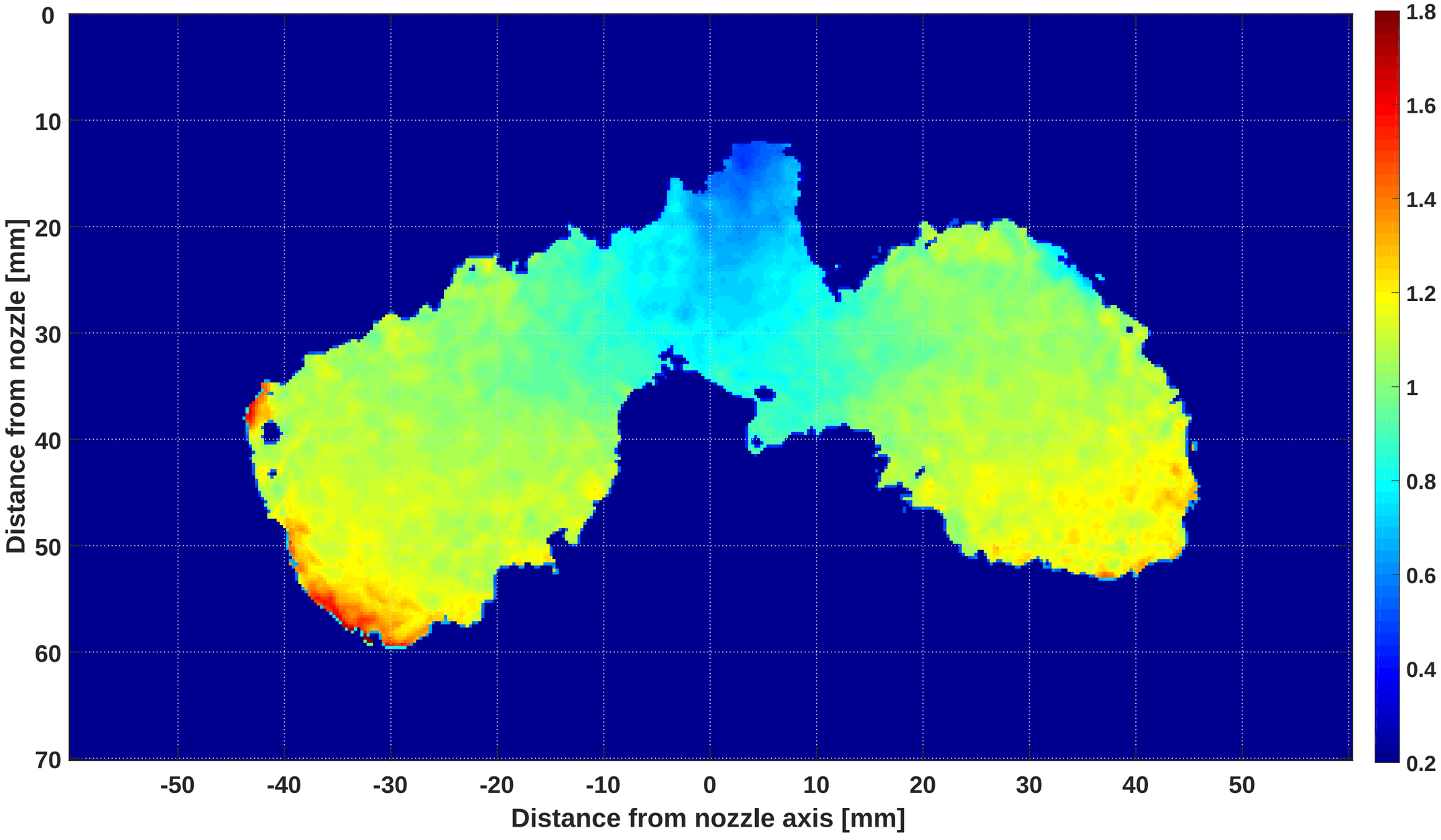
0
10
20
30
40
50
60
70
Distance from nozzle [mm]
-50
-40
-30
-20
-10
0
10
20
30
40
50
Distance from nozzle axis [mm]
1.8
1.6
1.4
1.2
1
0.8
0.6
0.4
0.2

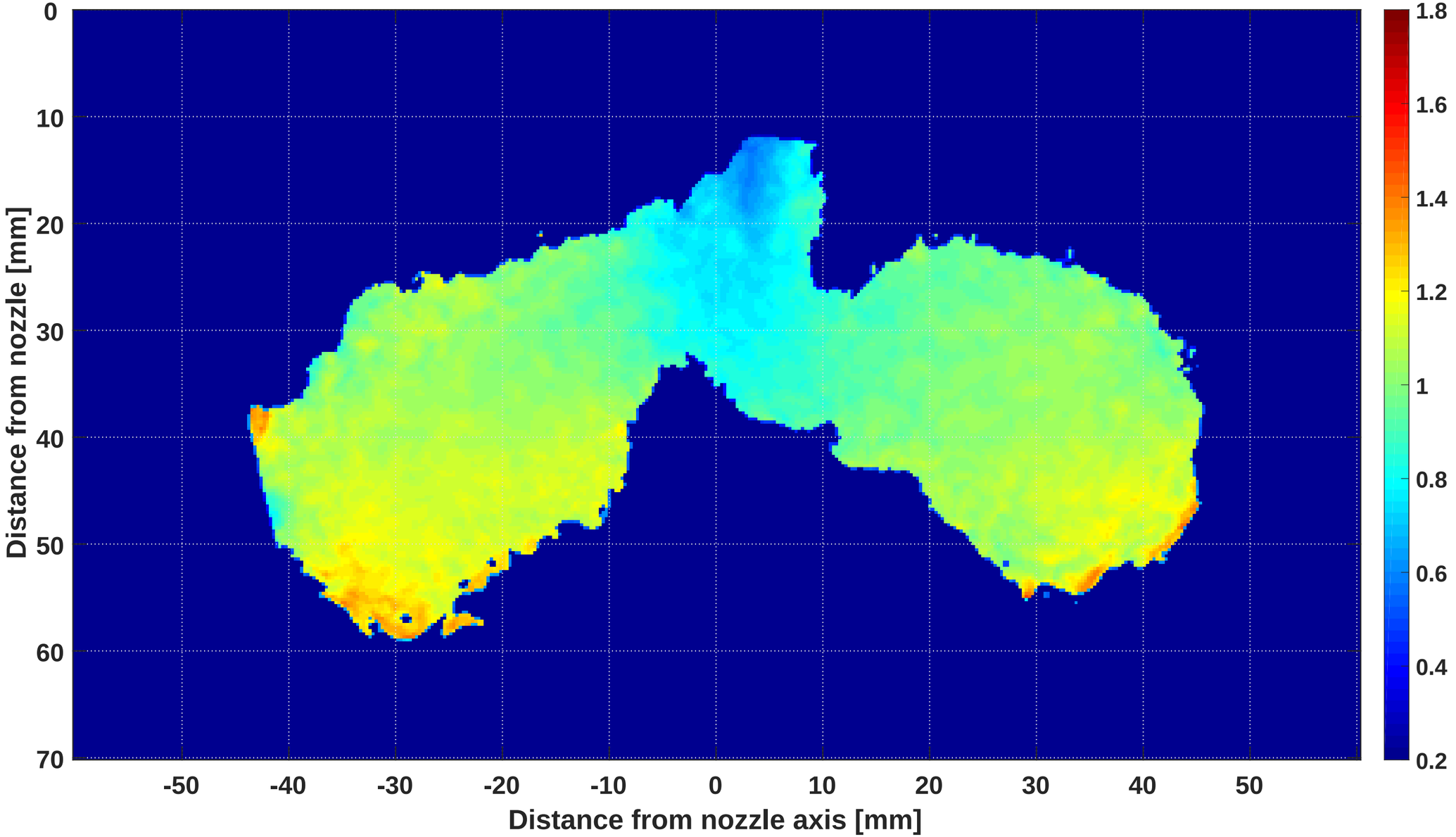
Distance from nozzle [mm]
0
10
20
30
40
50
60
70
-50
-40
-30
-20
-10
0
10
20
30
40
50
Distance from nozzle axis [mm]
1.8
1.6
1.4
1.2
1
0.8
0.6
0.4
0.2

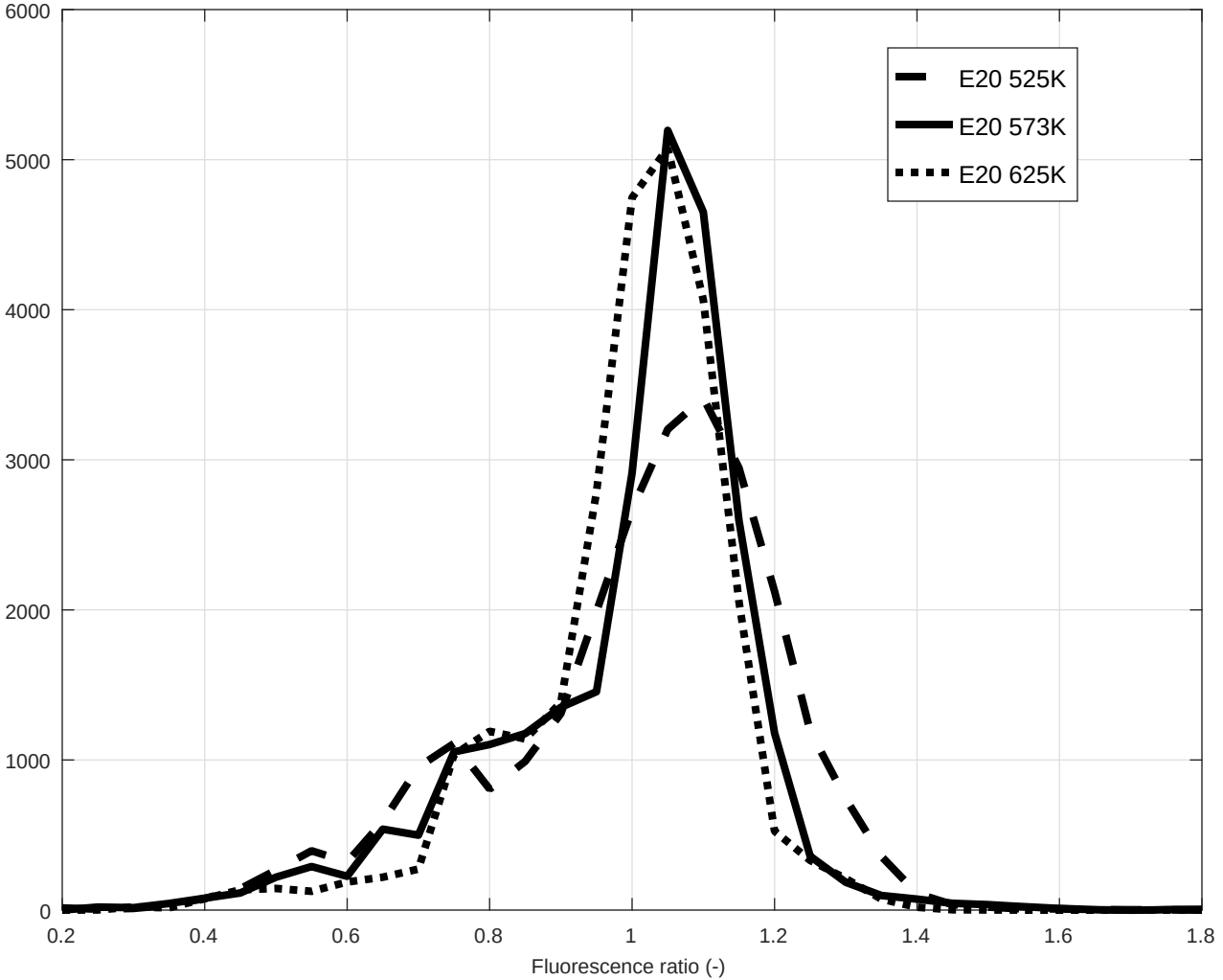
E20 525K
E20 573K
E20 625K
6000
5000
4000
3000
2000
1000
0
0.2
0.4
0.6
0.8
1
1.2
1.4
1.6
1.8
Fluorescence ratio (-)

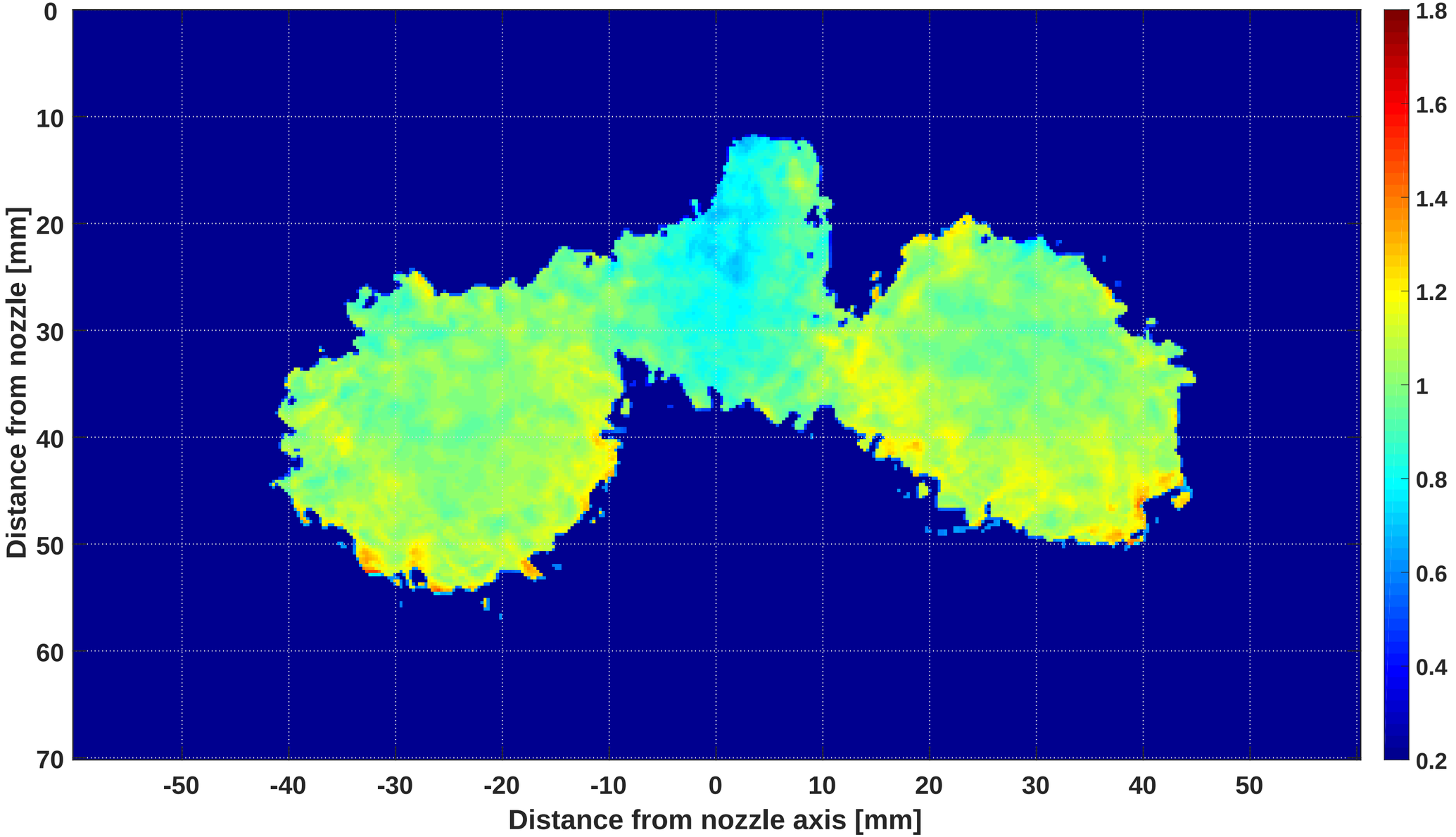
Distance from nozzle [mm]
0
10
20
30
40
50
60
70
-50
-40
-30
-20
-10
0
10
20
30
40
50
Distance from nozzle axis [mm]
1.8
1.6
1.4
1.2
1
0.8
0.6
0.4
0.2

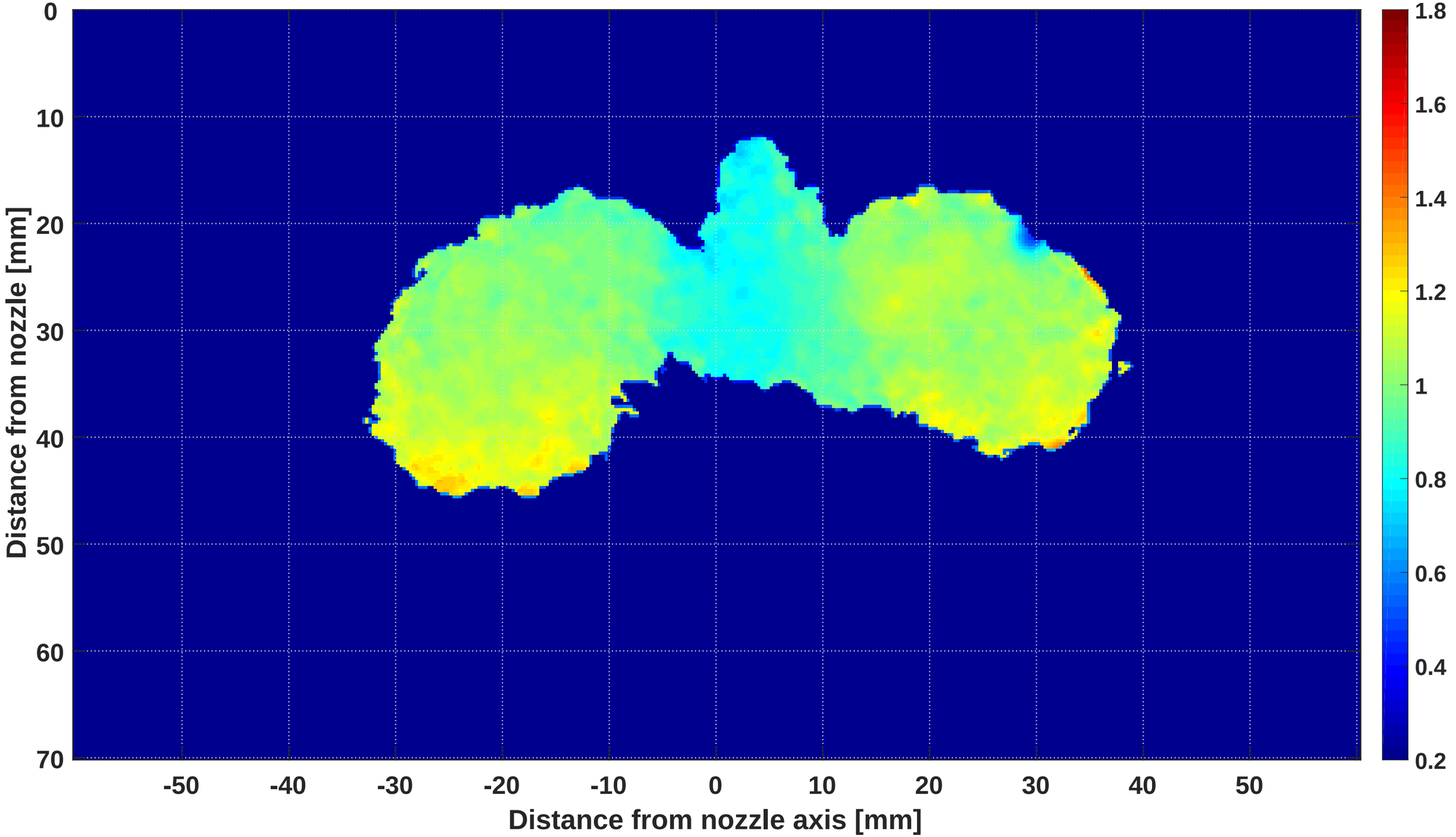
0
10
20
30
40
50
60
70
Distance from nozzle [mm]
-50
-40
-30
-20
-10
0
10
20
30
40
50
Distance from nozzle axis [mm]
1.8
1.6
1.4
1.2
1
0.8
0.6
0.4
0.2

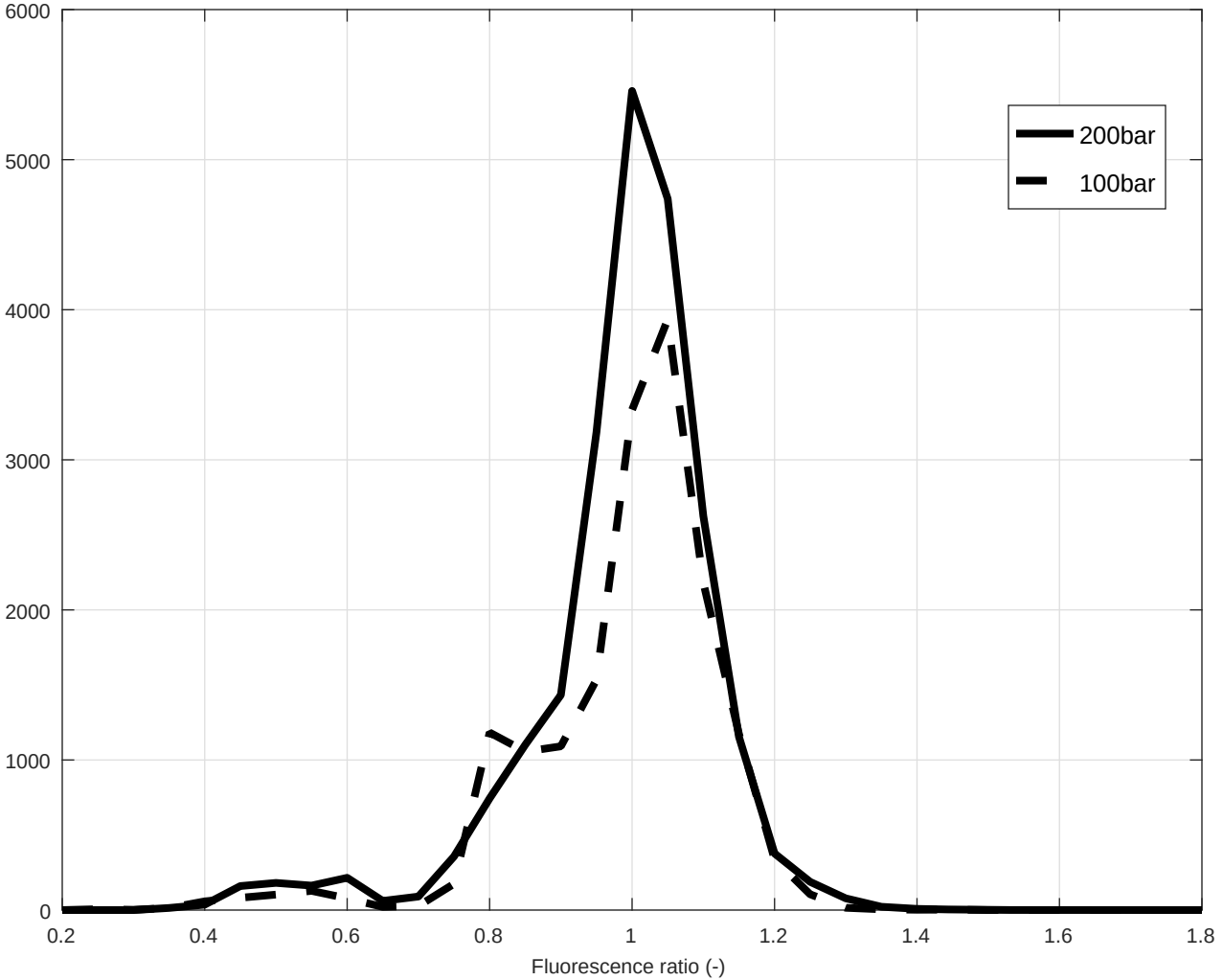
6000
5000
4000
3000
2000
1000
0
0.2
0.4
0.6
0.8
1
1.2
1.4
1.6
1.8
Fluorescence ratio (-)
200bar
100bar

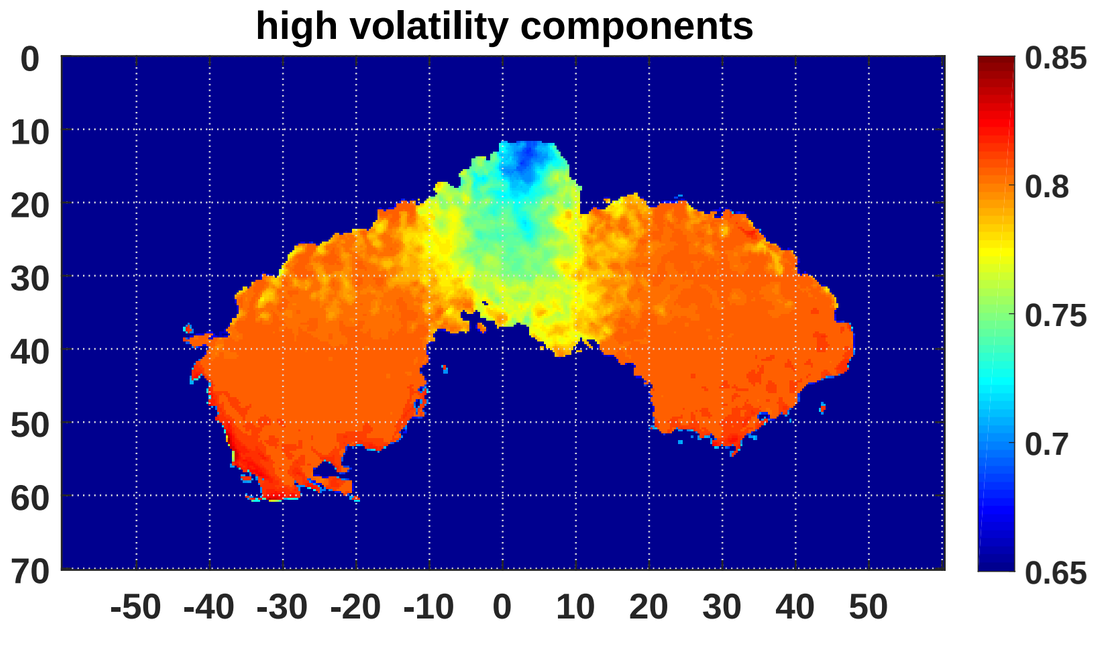
high volatility components
0
10
20
30
40
50
60
70
-50 -40 -30 -20 -10 0 10 20 30 40 50
0.85
0.8
0.75
0.7
0.65

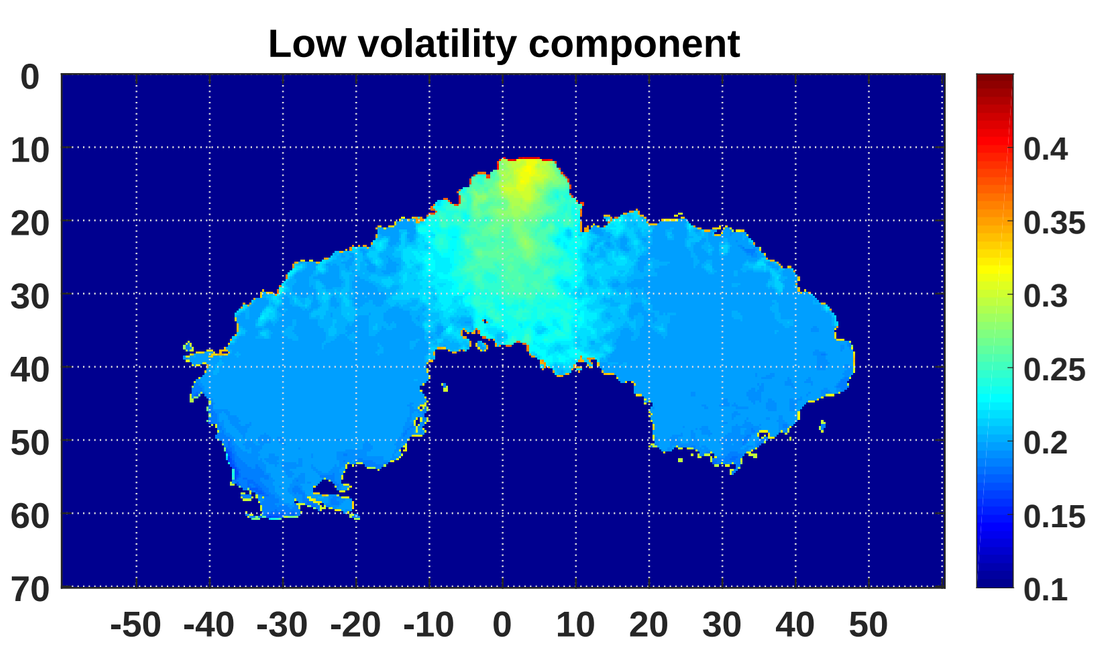
Low volatility component
0
10
20
30
40
50
60
70
-50 -40 -30 -20 -10 0 10 20 30 40 50
0.4
0.35
0.3
0.25
0.2
0.15
0.1

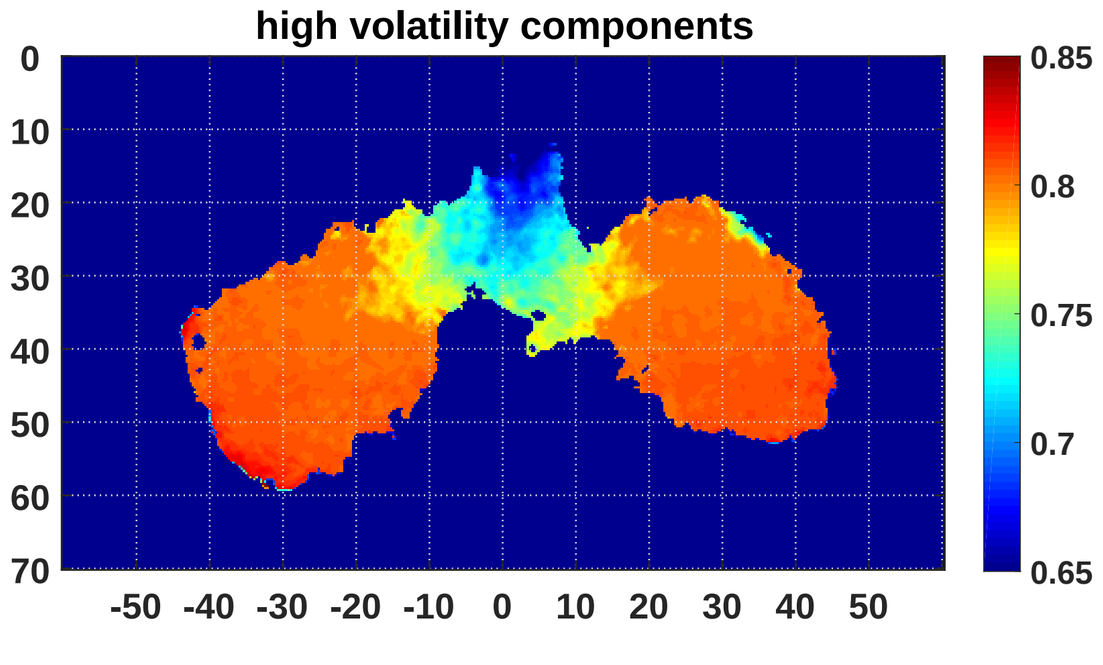
high volatility components
0
10
20
30
40
50
60
70
-50 -40 -30 -20 -10 0 10 20 30 40 50
0.85
0.8
0.75
0.7
0.65

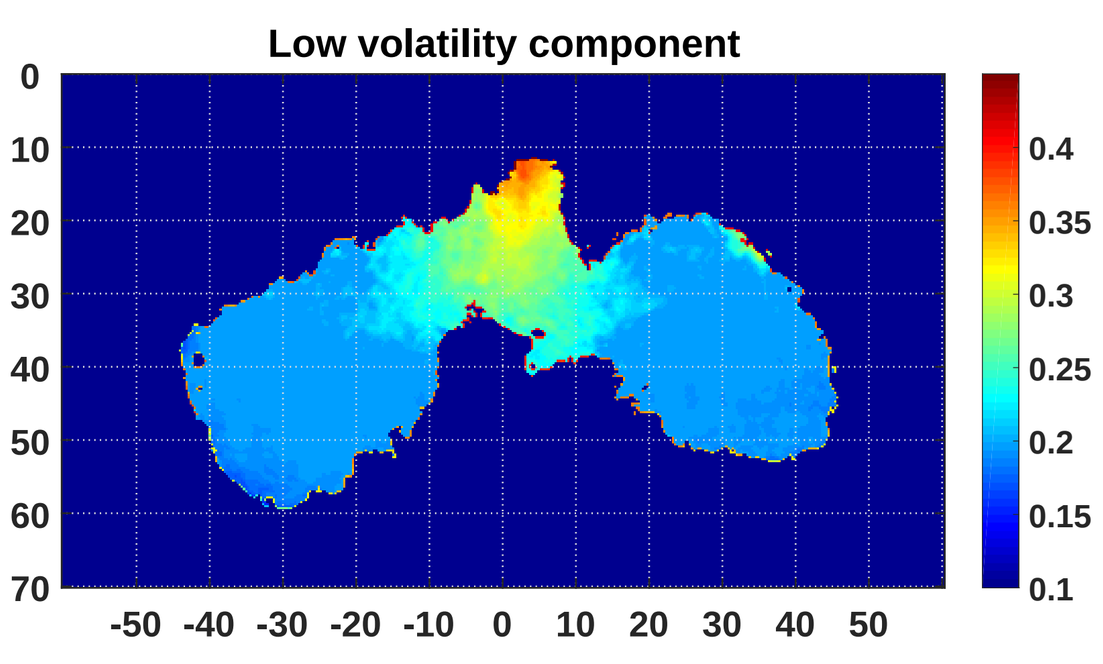
Low volatility component
0
10
20
30
40
50
60
70
-50 -40 -30 -20 -10 0 10 20 30 40 50
0.4
0.35
0.3
0.25
0.2
0.15
0.1

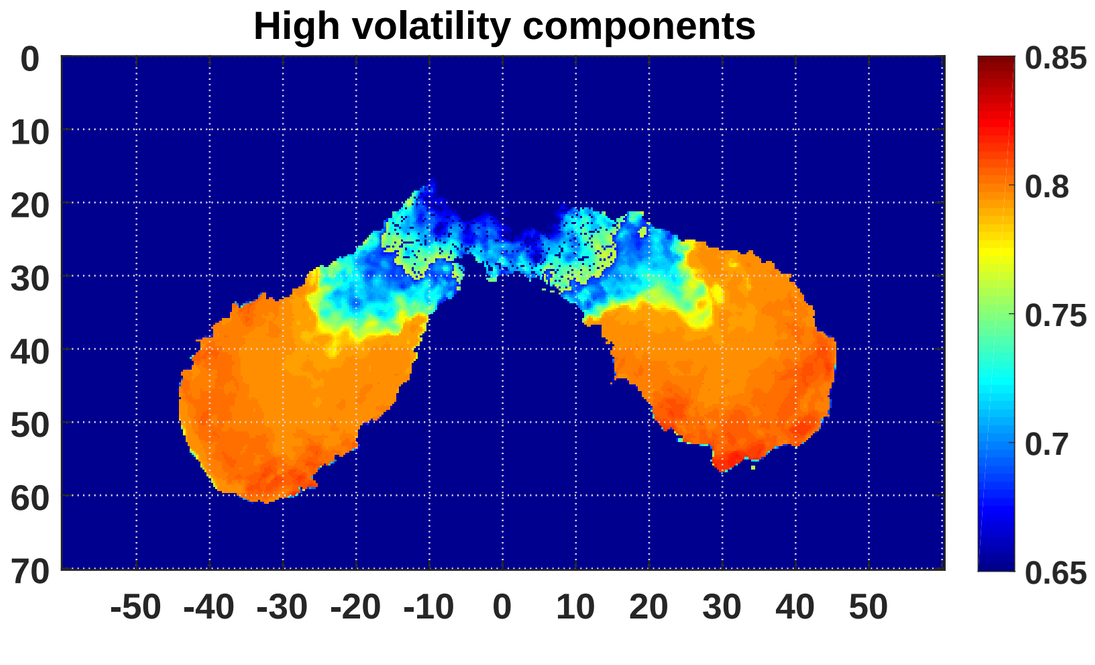
High volatility components
0
10
20
30
40
50
60
70
-50 -40 -30 -20 -10 0 10 20 30 40 50
0.85
0.8
0.75
0.7
0.65

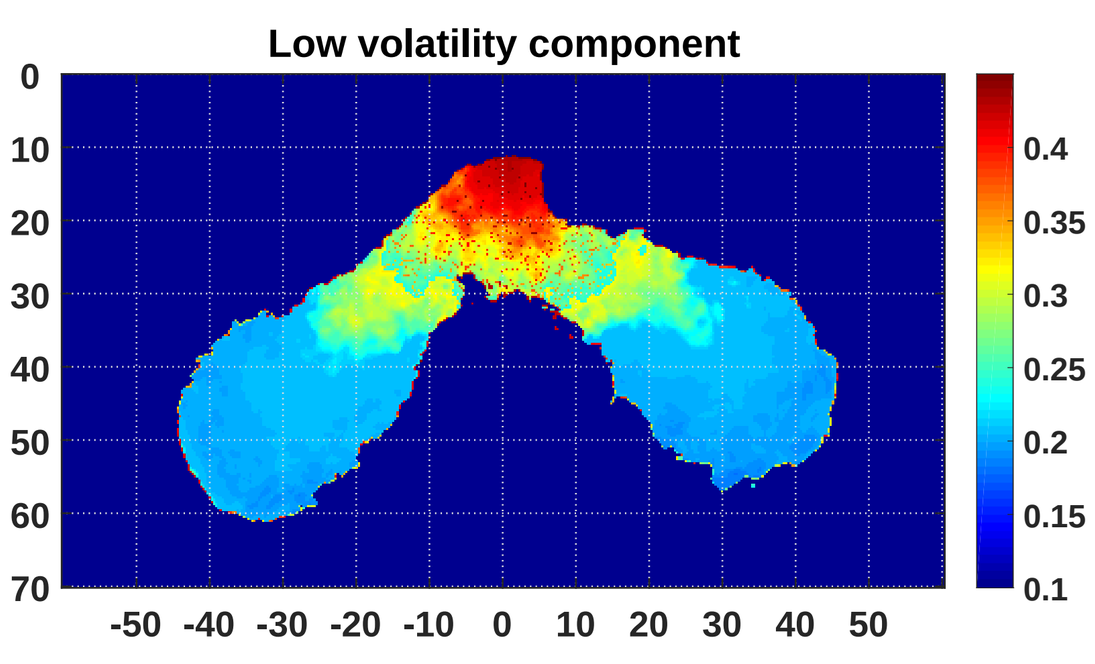
Low volatility component
0
10
20
30
40
50
60
70
-50 -40 -30 -20 -10 0 10 20 30 40 50
0.4
0.35
0.3
0.25
0.2
0.15
0.1